

University of Windsor

Scholarship at UWindor

Electronic Theses and Dissertations

Theses, Dissertations, and Major Papers

1-1-2006

Laboratory and production testing of novel resistance spot welding electrodes.

Jeremy Leonard Caron
University of Windsor

Follow this and additional works at: <https://scholar.uwindsor.ca/etd>

Recommended Citation

Caron, Jeremy Leonard, "Laboratory and production testing of novel resistance spot welding electrodes." (2006). *Electronic Theses and Dissertations*. 7095.
<https://scholar.uwindsor.ca/etd/7095>

This online database contains the full-text of PhD dissertations and Masters' theses of University of Windsor students from 1954 forward. These documents are made available for personal study and research purposes only, in accordance with the Canadian Copyright Act and the Creative Commons license—CC BY-NC-ND (Attribution, Non-Commercial, No Derivative Works). Under this license, works must always be attributed to the copyright holder (original author), cannot be used for any commercial purposes, and may not be altered. Any other use would require the permission of the copyright holder. Students may inquire about withdrawing their dissertation and/or thesis from this database. For additional inquiries, please contact the repository administrator via email (scholarship@uwindsor.ca) or by telephone at 519-253-3000ext. 3208.

**Laboratory and Production Testing of
Novel Resistance Spot Welding Electrodes**

by
Jeremy Leonard Caron

**A Thesis
Submitted to the Faculty of Graduate Studies and Research
through Engineering Materials
in Partial Fulfillment of the Requirements for
the Degree of Master of Applied Science at the
University of Windsor**

Windsor, Ontario, Canada

2006

© 2006 Jeremy Leonard Caron



Library and
Archives Canada

Bibliothèque et
Archives Canada

Published Heritage
Branch

Direction du
Patrimoine de l'édition

395 Wellington Street
Ottawa ON K1A 0N4
Canada

395, rue Wellington
Ottawa ON K1A 0N4
Canada

Your file *Votre référence*

ISBN: 978-0-494-35956-3

Our file *Notre référence*

ISBN: 978-0-494-35956-3

NOTICE:

The author has granted a non-exclusive license allowing Library and Archives Canada to reproduce, publish, archive, preserve, conserve, communicate to the public by telecommunication or on the Internet, loan, distribute and sell theses worldwide, for commercial or non-commercial purposes, in microform, paper, electronic and/or any other formats.

The author retains copyright ownership and moral rights in this thesis. Neither the thesis nor substantial extracts from it may be printed or otherwise reproduced without the author's permission.

AVIS:

L'auteur a accordé une licence non exclusive permettant à la Bibliothèque et Archives Canada de reproduire, publier, archiver, sauvegarder, conserver, transmettre au public par télécommunication ou par l'Internet, prêter, distribuer et vendre des thèses partout dans le monde, à des fins commerciales ou autres, sur support microforme, papier, électronique et/ou autres formats.

L'auteur conserve la propriété du droit d'auteur et des droits moraux qui protègent cette thèse. Ni la thèse ni des extraits substantiels de celle-ci ne doivent être imprimés ou autrement reproduits sans son autorisation.

In compliance with the Canadian Privacy Act some supporting forms may have been removed from this thesis.

Conformément à la loi canadienne sur la protection de la vie privée, quelques formulaires secondaires ont été enlevés de cette thèse.

While these forms may be included in the document page count, their removal does not represent any loss of content from the thesis.

Bien que ces formulaires aient inclus dans la pagination, il n'y aura aucun contenu manquant.


Canada

ABSTRACT

The performance of two novel resistance spot welding electrodes was evaluated through the General Motors WS-5A laboratory test and production trials in an automotive assembly plant. The novel electrodes featured enhanced cooling properties such as a reduced face thickness and internal fins. The potential for a multiple-oxide dispersion strengthened copper electrode material is revealed given its performance in both the laboratory and production testing. For the production trials, extended electrode life and lower current levels were achieved compared to the baseline electrode. The results suggest that the optimum face thickness for electrode cooling is greater than 6 mm for a cooling-water flow rate of 0.5 gpm. The results also indicate that increased cooling-water flow rate is more beneficial for electrodes with cooling properties that enhance convective heat transfer. A methodology is presented for developing weld schedules in production operations.

DEDICATION

I dedicate this thesis to my parents, who have always encouraged me to strive for excellence.

ACKNOWLEDGEMENTS

First and foremost I would like to thank my advisor Dr. Randy Bowers for his guidance during my graduate studies. He was a motivating force in my decision to pursue an advanced degree and is commended for his ability to simplify the learning process. I would also like to thank Morgan Gallagher and Bobby Athwal, whose initial work on the project provided a basis for this thesis.

I would like to acknowledge the other members of the project team, specifically Warren Peterson and Eric Pakalnins. Without their technical expertise and leadership, this project would not have been possible. Warren's immense knowledge of resistance spot welding and his extensive literature review of electrode wear proved to be invaluable sources of information. Eric's project management skills ensured that the production trials were carried through to their conclusion.

Thanks are sent out to Brad Chrichton, Frank Pavicic, and Kathy Stergianis for coordinating the production trials at the DaimlerChrysler Windsor Assembly Plant. The assistance of the various electricians, weld techs, and destruct personnel is also saluted. The efforts of Michael Karagoulis are gratefully appreciated for organizing the laboratory tests at the General Motors Technical Center. Special thanks are also extended to John Robinson for his assistance in the metallographic preparation of the electrodes.

The financial support of the United States Council for Automotive Research (USCAR), the Natural Sciences and Engineering Research Council of Canada (NSERC), and the University of Windsor are graciously acknowledged.

TABLE OF CONTENTS

ABSTRACT.....	iii
DEDICATION.....	iv
ACKNOWLEDGEMENTS.....	v
LIST OF TABLES.....	viii
LIST OF FIGURES.....	ix
LIST OF ABBREVIATIONS.....	xii
I. INTRODUCTION.....	1
II. LITERATURE REVIEW.....	3
2.1 The Resistance Spot Welding Process.....	3
2.1.1 Resistance Heat Generation.....	4
2.1.2 The Resistance Spot Welding Cycle.....	5
2.1.3 The Weld Lobe Curve.....	5
2.2 Electrodes.....	7
2.2.1 Electrode Materials.....	7
2.1.2 Electrode Geometry.....	9
2.3 Laboratory Test Methods.....	10
2.3.1 AWS Endurance Test.....	11
2.3.2 GM Stepper Test.....	12
2.3.3 Oscillating Weldability Lobe Test.....	12
2.3.4 Sequential Life Test.....	12
2.4 Production Welding.....	13
2.4.1 Production-Specific Issues.....	13
2.4.2 Methods to Extend Electrode Life in Production.....	14
2.5 Galvanized Steel in the Automotive Industry.....	15
2.5.1 Types of Galvanized Coatings.....	15
2.5.2 Resistance Spot Welding of Galvanized Steel.....	16
2.5.3 Galvanized Steel and Electrode Life.....	17
2.5.3.1 Hot-Dipped Galvanized Coatings and Electrode Life.....	18
2.5.3.2 Galvannealed Coatings and Electrode Life.....	18
2.6 Electrode Wear Mechanisms for Galvanized Steel.....	19
2.6.1 Brass-Alloy Formation on the Electrode Face.....	19
2.6.2 Electrode Face Enlargement.....	21
2.6.2.1 Brass-Alloy Extrusion.....	21
2.6.2.2 Bulk Copper Extrusion.....	21
2.6.3 Sticking and Brassing.....	21
2.6.4 Pitting and Cavitation.....	22

2.6.5 Cracking	23
2.6.6 Protrusions	23
2.6.7 Electrode Wear Sequence	24
III. EXPERIMENTAL MATERIALS AND PROCEDURE.....	25
3.1 Electrode Properties	25
3.2 GM Stepper Tests Procedure	27
3.3 DCX Beta-Site Trials Procedure.....	29
3.4 Metallographic Procedure	31
3.5 Alloy Layer Thickness Measurements.....	33
3.6 Hardness Measurements	33
IV. EXPERIMENTAL RESULTS	34
4.1 GM Stepper Tests Results.....	34
4.2 DCX Beta-Site Trials Results	37
4.2.1 Current Range Results	37
4.2.2 Expulsion Observations - M Electrode	38
4.2.3 Expulsion Observations - FIN Electrode	41
4.2.4 Expulsion Observations - WAP Electrode.....	44
4.3 Electrode Face Images	47
4.4 Metallographic Evaluation.....	54
4.4.1 Microhardness Results	54
4.4.2 Alloy Layer Thickness Measurements.....	57
4.4.3 Microstructural Observations.....	60
V. DISCUSSION	63
5.1 Comparison of Test Results	63
5.2 Electrode Face Enlargement	64
5.3 Current Density Requirements.....	65
5.4 The Importance of Electrode Cooling.....	66
5.5 Candidate Electrode Material	69
5.6 Evolutionary Operation of Weld Schedules.....	70
5.7 Benefits of Evolutionary Operation	74
VI. CONCLUSIONS AND FUTURE WORK.....	76
REFERENCES	78
VITA AUCTORIS	83

LIST OF TABLES

Table 1: Properties of RWMA materials	9
Table 2: Iron-zinc alloy compositions in a hot-dipped galvanized coating	16
Table 3: Composition and geometry alterations for each of the tested electrodes	26
Table 4: Chemical composition, coating properties, and mechanical properties of the hot-dipped galvanized sheet steel used for the GM stepper tests.....	28
Table 5: Weld parameters for the GM stepper tests	28
Table 6: Weld parameters for the DCX beta-site trials.....	30
Table 7: Line of best-fit equations and R^2 values for the GM stepper tests	35
Table 8: Summary of electrode face diameters (mm) for the GM stepper tests	49
Table 9: Summary of electrode face diameters (mm) for the DCX beta-site trials	49
Table 10: Rate of electrode face diameter increase for each testing condition.....	64
Table 11: End-of-life current density comparison	66
Table 12: Summary of weld currents and total amperes for the DCX beta-site trials	75

LIST OF FIGURES

Figure 1: Resistance spot welding setup.....	3
Figure 2: Major points of heat generation and temperature gradients after 20 and 100% of weld time	4
Figure 3: Single-impulse resistance spot welding cycle.....	5
Figure 4: Development of a weld lobe curve.....	7
Figure 5: Standard electrode geometries.....	10
Figure 6: Measuring button size from a peel-test sample.....	11
Figure 7: The copper-zinc phase diagram.....	20
Figure 8: Female B-nose electrode used for the testing.....	26
Figure 9: Sectioned view of the FIN electrode showing the fins in the water channel	26
Figure 10: Carbon imprint schematic	29
Figure 11: (a) Electrode sectioning schematic and (b) final mount sample showing the location of the microstructural observations	32
Figure 12: GM stepper tests results on hot-dipped galvanized steel showing the weld current vs. weld number data and line of best-fit for each electrode	35
Figure 13: GM stepper test button size measurements for the CuZr electrode.....	36
Figure 14: GM stepper test button size measurements for the M electrode	36
Figure 15: GM stepper test button size measurements for the FIN electrode.....	37
Figure 16: Button size measurements for the DCX beta-site trials current range test.....	38
Figure 17: Expulsion observations for the preliminary M electrode trials	39
Figure 18: Expulsion observations for the M electrode trials conducted with an 8500 A start current and 0.75A per weld stepper rate.....	40
Figure 19: Expulsion observations for the M-12hr trials.....	40
Figure 20: Expulsion observations for the preliminary FIN electrode trials	41

Figure 21: Expulsion observations for the FIN-12hr trials	42
Figure 22: Expulsion observations for the FIN-24hr trial.....	43
Figure 23: Baseline expulsion observations for the WAP electrode	45
Figure 24: Expulsion observations for the preliminary WAP electrode trials.....	45
Figure 25: Expulsion observations for the WAP electrode trials conducted with an 8500 A start current and 0.65, 0.75, 0.85 A per weld stepper schedule	46
Figure 26: GM stepper tests end-of-life electrode face images	48
Figure 27: Electrode face images for the M electrode trials	50
Figure 28: Electrode face images for the FIN electrode trials	51
Figure 29: Electrode face images for the WAP electrode trials.....	53
Figure 30: Hardness values at the face centre for the GM stepper tests electrodes.....	55
Figure 31: Hardness values at the face edge for the GM stepper tests electrodes	55
Figure 32: Hardness values at the face centre for the DCX beta-site trials electrodes	56
Figure 33: Hardness values at the face edge for the DCX beta-site trials electrodes	56
Figure 34: Alloy layer thickness measurements for both the GM stepper tests electrodes and the DCX beta-site trials electrodes.....	58
Figure 35: Optically distinct beta-brass (yellow), gamma-brass (white), and parting layers in the FIN-24 electrode.....	59
Figure 36: Mixing of the parting and gamma-brass layers in a FIN-12 electrode.....	59
Figure 37: Recrystallization at the centre of the electrode face for the FIN-24 electrode	61
Figure 38: Deformation pattern of an M-12 electrode which shows no evidence of recrystallization at the edge of the electrode face.....	61
Figure 39: A double crack intersecting a central pit in an M-12 electrode.....	62
Figure 40: Extensive wing formation in a FIN-12 electrode showing both brass-alloy extrusion and copper extrusion at the edge of the electrode face	62

Figure 41: An untested M electrode (l) and one exhibiting white residue from boiled cooling-water (r)..... 68

Figure 42: An upclose (29.5X) of the white residue found on the inside face of the M electrode..... 68

Figure 43: A 2² factorial design for variables start current and stepper rate 71

Figure 44: Progression of the factorial design for the example welding application 73

Figure 45: Graph of weld current vs. weld number for the final weld schedules..... 75

LIST OF ABBREVIATIONS

AWS	American Welding Society
DCX	DaimlerChrysler Corporation
DSC	Dispersion Strengthened Copper
EG	Electrogalvanized
EVOP	Evolutionary Operation
FIN	Novel electrode (see page 26)
GA	Galvannealed
GM	General Motors Corporation
gpm	gallons per minute
HDG	Hot-Dipped Galvanized
HRB	Rockwell Hardness B
HSLA	High Strength Low Alloy
HV	Vickers Hardness
IACS	International Annealed Copper Standard
M	Novel electrode (see page 26)
NSERC	Natural Sciences and Engineering Research Council of Canada
ODS	Oxide Dispersion Strengthened
PDC	Passive Data Collection
RSW	Resistance Spot Welding
RWMA	Resistance Welder Manufacturers' Association
USCAR	United States Council for Automotive Research
WAP	Baseline electrode for DCX beta-site trials
WPM	Welds per Minute

I. INTRODUCTION

The Resistance Spot Welding (RSW) process is the primary method for joining automotive assemblies in mass production. Its relatively low capital and operating costs along with its capacity to support high production rates continue to make the process very attractive to the automotive industry. However, advancements in the primary materials used in vehicle assembly have had a significant impact on weld process robustness and weld quality.

The demand for improved automobile performance and efficiency has led to the production of new base metals, coatings, and treatments. Galvanized coatings were introduced to the automotive industry for their increased corrosion resistance properties. The copper-based electrodes, which contact the workpiece and deliver the weld current, alloy with the galvanized coating causing undesirable changes in their electrical, thermal, and mechanical properties. Furthermore, the electrodes are subjected to great compressive stresses at elevated temperatures leading to electrode face enlargement. This electrode wear process requires replacement of the electrodes within a small fraction of the life that would be attainable on uncoated steel, and results in reduced weld quality reliability. Electrode wear also adversely affects the cost and productivity of automotive assembly by requiring intensified inspection requirements and stricter control of weld parameters.

Automotive companies alleviate the effects of electrode wear by systematically increasing the weld current or by reconditioning the electrode face. Current stepping and electrode dressing have been used for many years on galvanized steels to increase electrode life; however, these techniques do not address the underlying causes of electrode wear. New electrode materials and geometries are needed to achieve a significant increase in electrode life and the concomitant cost reduction and weld quality improvement.

In a production environment, electrodes are normally replaced during breaks, at lunch, or between shifts. Thus, improvements in electrode life must be consistent with production scheduling in order to reap any significant economic gain. The annual savings associated with doubling electrode life, based only on electrode costs and

replacement labour, was estimated in 2002 to be \$US 20-million for the three North American automakers alone [1]. However, increased electrode life for the resistance spot welding of galvanized steel continues to be a significant challenge for the automotive industry.

In an effort to extend electrode life on galvanized steel consistent with production scheduling, a research initiative began under the direction of the United States Council for Automotive Research (USCAR). The initial stages of the research work set out to survey and comparatively test a broad selection of existing and developing technologies with technical merit for achieving long electrode life. A detailed characterization of the electrode wear process was obtained through a combination of laboratory testing, metallography, and computer modeling. For the final stage of the research initiative, the electrode designs offering the best opportunity for enhanced electrode life were beta-site tested in an automotive assembly plant. The selection process was based on previous laboratory results, a working knowledge of automotive production facilities, and the review of industry experts [2].

The main objective of this study was to evaluate the production welding performance of two novel resistance spot welding electrodes. The research approach was to generate a methodology for developing weld schedules in production operations. Another objective of this study was to compare and contrast the results from the laboratory testing to the results obtained from the production trials.

II. LITERATURE REVIEW

The following literature review serves to introduce the fundamentals of resistance spot welding for those that are unacquainted with the process. It also highlights the various electrode materials and geometries, and describes several laboratory test methods that are used to evaluate electrode performance. Production-specific welding issues are discussed along with the methods used to extend electrode life. Information about galvanized coatings is presented along with their resistance spot welding characteristics. Finally, a detailed analysis of the various electrode wear mechanisms for galvanized steel is provided.

2.1 The Resistance Spot Welding Process

Resistance welding is a process in which heat is generated in workpieces from the resistance to the flow of electric current [3]. The resistance welding phenomenon was first discovered by Elihu Thomson in 1877 [4]. Resistance spot welding is one type of resistance welding process whereby two or more thin sheets of metal are joined at their contacting, or faying, surfaces by electrodes that provide current and force. The faying surfaces in the region of current concentration are heated by a pulse of low-voltage, high-amperage current to form a nugget of weld metal [3]. A sectioned view of the resistance spot welding setup is shown in Figure 1 displaying the shape of the nugget and the position of the nugget relative to the inner and outer surfaces of the workpieces.

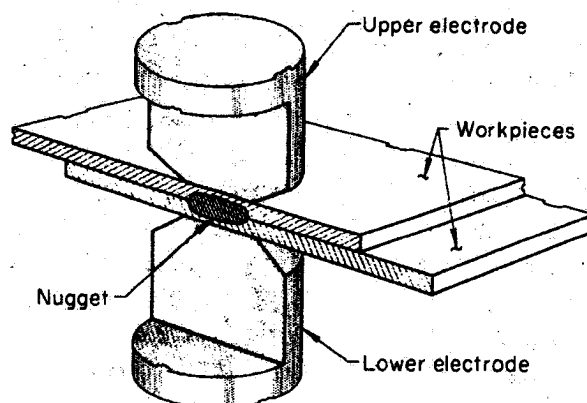


Figure 1: Resistance spot welding setup [5]

2.1.1 Resistance Heat Generation

Heat is generated when an electric current passes through a resistance. The two types of resistances present in the welding circuit are the volume resistances of the workpieces and the interfacial resistances of the contacting surfaces. The heat energy generated at any point is given by Joule's Law: $Q = I^2 R t$

Q = heat generated (joules) I = current (amperes)

R = resistance (ohms) t = duration of current (seconds)

The current flow through all parts of the circuit is the same at any point regardless of the resistance. The major points of heat generation and temperature gradients after 20 and 100% of weld time are shown in Figure 2. Part of the heat generated is used to make the weld while the remainder is lost to the surrounding metal and water-cooled electrodes. The seven resistances connected in series are: (a) the bulk resistance of the upper electrode; (b) the contact resistance between the upper electrode and the upper workpiece; (c) the bulk resistance of the upper workpiece; (d) the interfacial contact resistance between the upper and lower workpieces; (e) the bulk resistance of the lower workpiece; (f) the contact resistance between the lower electrode and the lower workpiece; and (g) the bulk resistance of the lower electrode. The point of highest resistance, where heating is localized sufficiently to cause melting, is at the faying interface [3, 5].

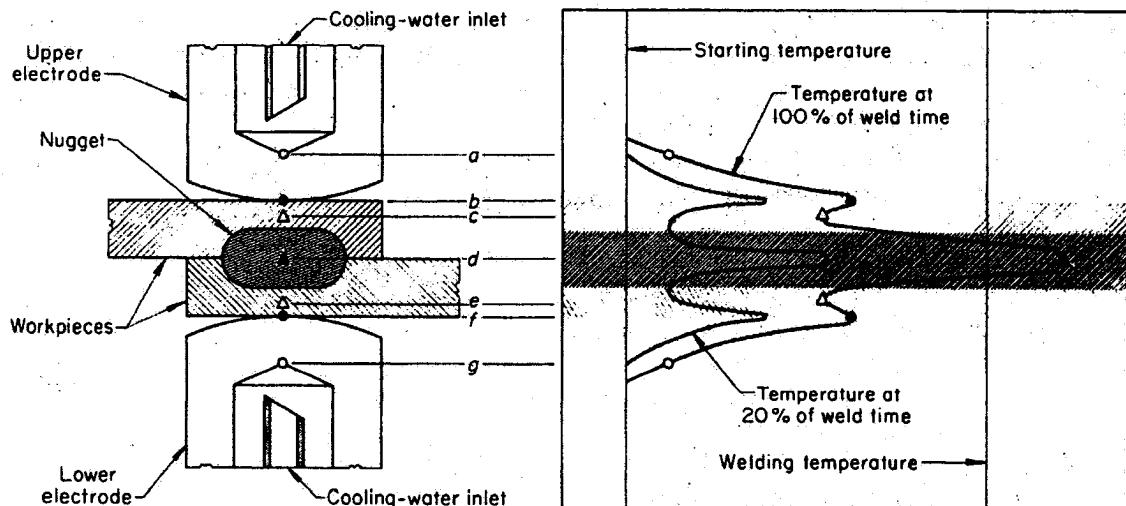


Figure 2: Major points of heat generation and temperature gradients after 20 and 100% of weld time [5]

2.1.2 The Resistance Spot Welding Cycle

The resistance spot welding cycle consists of a sequence of both current and force during the formation of a weld. Figure 3 displays the single-impulse resistance spot welding cycle. The four basic steps of the cycle are:

1. Squeeze time - electrodes clamp the workpieces together to apply a force
2. Weld time - weld current is initiated and maintained as the weld is created
3. Hold time - weld current is turned off as electrode force is maintained until the weld nugget solidifies
4. Off time - the electrodes open to allow the workpieces to be moved into position for the next weld

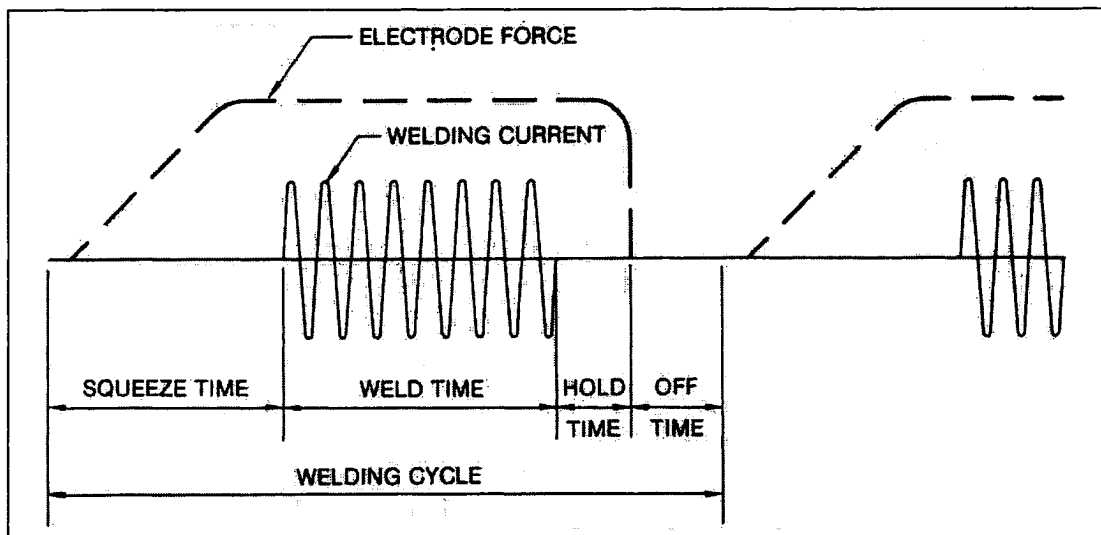


Figure 3: Single-impulse resistance spot welding cycle [3]

2.1.3 The Weld Lobe Curve

The major parameters that affect the resistance spot welding process are weld current, weld time, and electrode force. Many combinations of the above parameters will produce an acceptable weld nugget size.

Figure 4(a) schematically illustrates nugget diameter as a function of weld current for a specific weld time. The minimum nugget diameter is generally established by specification. As the current is increased, the nugget diameter increases up to and, in

most cases, beyond the *expulsion* level. Expulsion is defined as the ejection of molten weld metal from between the workpieces. Expanding the acceptable range by testing at other weld times produces a weld lobe curve, which defines the combination of weld currents and times over which acceptable nuggets are produced [5]. The width of the weld lobe curve is known as the *current range*. The current range can be taken as a measure of the weldability of the workpieces. Weldability is a comparative term that is loosely defined as the capacity of a material to be welded under the fabrication conditions imposed [5]. Materials that have wide weld lobe curves and produce repeatable acceptable welds are considered to have good weldability.

Weld current must be sufficient enough for heat to accumulate faster than it dissipates so that fusion can occur. The threshold current value must be such that it produces enough heat to bring the faying interface to a plastic temperature in spite of heat losses by conduction and radiation [3]. Lower current levels produce undersized, brittle welds because the nugget is produced at lower peak temperatures, and remains above the melting point for shorter periods of time [6]. Current levels that are too high may heat the entire thickness of the workpiece into the plastic region causing excess indentation on the sheet surface and expulsion of weld metal [3].

Weld times need to be carefully considered in relation to weld current. Shorter weld times require higher weld currents in order to produce a weld nugget. Since heat transfer is time dependent, weld time can only be shortened to a certain extent regardless of the increase in current [3].

Electrode force plays an important role in the size and location of the weld lobe curve. Electrode force should be such that it holds the workpieces tightly both to allow the passage of current during the weld time, as well as to ensure weld nugget solidification during the hold time. Increasing the electrode force decreases the contact resistance of the workpieces, thereby reducing the heat generated at the faying interface. Thus, electrode force should be selected so that excessive current is not required to generate a weld [5, 6].

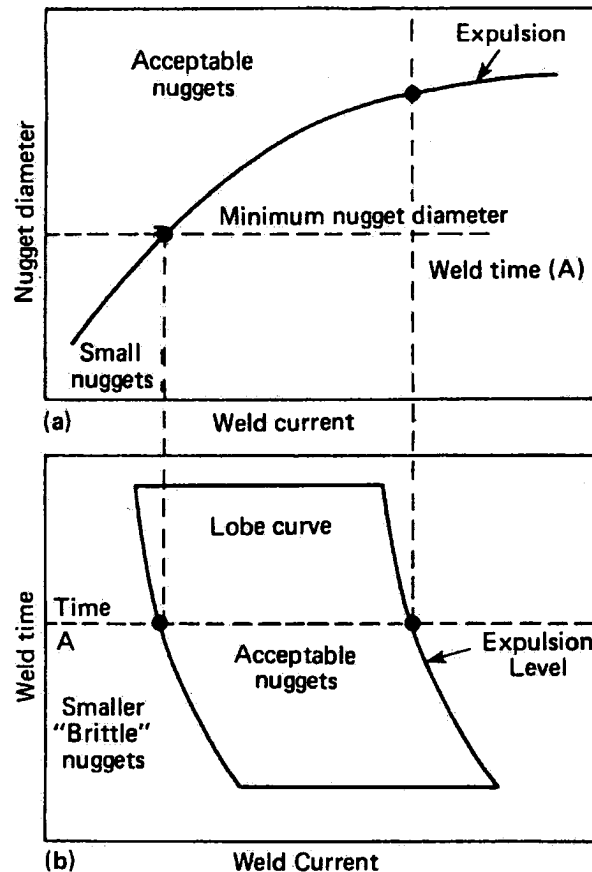


Figure 4: Development of a weld lobe curve [5]

2.2 Electrodes

Resistance spot welding electrodes are the component that contacts the workpieces and carries current to create the weld. Electrodes perform three important functions [3, 5]:

1. Conduct welding current to the workpieces;
2. Transmit the applied force to the workpieces;
3. Dissipate heat away from the weld zone.

2.2.1 Electrode Materials

A suitable electrode material must have high electrical conductivity to carry the weld current to the workpiece and high thermal conductivity to conduct heat away from

the weld zone to aid nugget solidification. Electrodes must also have adequate high-temperature strength to resist mechanical deformation caused by the repeated application of electrode force.

Electrode materials are categorized by the Resistance Welder Manufacturers' Association (RWMA) into groups A, B, and C, as shown in Table 1 [3]. RWMA Group A materials consist of copper alloys that attain their strength from a combination of heat treatment and cold working. Group A, Class 1 materials have the highest electrical conductivities and are recommended for welding aluminum alloys, magnesium alloys and coated materials. Class 1 materials include copper-zirconium (CuZr) and copper-cadmium (CuCd) alloys.

Group A, Class 2 materials have slightly lower electrical conductivity and higher mechanical properties than Class 1 materials. Class 2 materials are general purpose electrode materials that can be used with a wide range of metals and conditions. Class 2 materials include copper-chromium (CuCr) and copper-chromium-zirconium (Cu-Cr-Zr) alloys.

Group A, Class 3 materials possess higher hardness and lower electrical conductivity than Class 1 or Class 2 materials. They are used for the most severe welding conditions since they have high annealing temperatures and good wear resistance. They are ideal for spot welding high resistance materials such as stainless steel, nichrome, and monel metal. Alloys in this group include copper-beryllium-nickel (Cu-Be-Ni) and copper-beryllium-cobalt (Cu-Be-Co).

Group B electrode materials consist of pressed and sintered powdered refractory metal compositions. They are divided into classes 10 to 14 and are recommended where high resistance to deformation is paramount to electrical conductivity. These electrode materials are used where high heat, long weld time, inadequate cooling, or high pressure would cause rapid deterioration of the copper-based alloys [3].

Group C electrode materials are special alloys that are neither solid solution copper alloys nor refractory metal compositions. Group C, Class 20 materials are dispersion-strengthened copper (DSC) alloys produced from powder metallurgy. The most widely used Class 20 material consists of pure copper containing finely dispersed particles of aluminum oxide (Al_2O_3). The oxide particles act as barriers to dislocation

motion and retard recrystallization of the copper. Class 20 electrodes have excellent high temperature strength and are recommended for welding coated materials.

RWMA Group	Class	Compositions	HRB	Minimum Electrical Conductivity (%IACS)
A	1	CuZr, CuCd	55-65	80
	2	CuCr, Cu-Cr-Zr	65-75	75
	3	Cu-Be-Co, Cu-Be-Ni	90	45
	4	CuBe	33 HRC	20
	5	CuAl	88	12
B	10	45Cu-55W	72	45
	11	25Cu-75W	94	40
	12	20Cu-80W	98	35
	13	Tungsten	69 HRA	30
	14	Molybdenum	85	30
C	20	Cu + 0.5- 1.1% Al ₂ O ₃	65-75	75

Table 1: Properties of RWMA materials [3]

2.2.2 Electrode Geometry

Electrode geometry is a significant aspect of the resistance spot welding process. The appropriate selection of electrode geometry is controlled by the specific application. Figure 5 illustrates the most common electrode geometries. The most commonly used electrodes for general welding applications are types A, B, and E. D-nose electrodes are necessary when a weld has to be made close to an upturned flange or corner. The particular electrode geometry that is selected in industry is often dictated by the part fit-up. Generally, flat-face electrodes are selected when there is good fit-up while radius-face electrodes provide the best service when there is poor fit-up.

Electrodes are equipped with water cooling channels to extract heat from the electrode and workpieces. Heat from the welding process is conducted through the electrode and is coupled with the cooling-water. The size of the cooling channel, the

position of the cooling tubes, and the distance between the electrode face and the water channel, known as the *face thickness*, are critical components for efficient cooling.

The electrode face diameter is an important consideration for producing quality welds. Electrode face diameter is governed by the thickness of the workpieces and the desired size of weld nugget [5]. *Current density*, defined as welding current divided by the contact area of the electrode face, is directly affected by electrode face diameter. If the electrode face diameter is too small, a high current density may cause severe heat concentration and excessive surface indentation. When the electrode face diameter is too large, current density drops below the minimum required to make a weld.

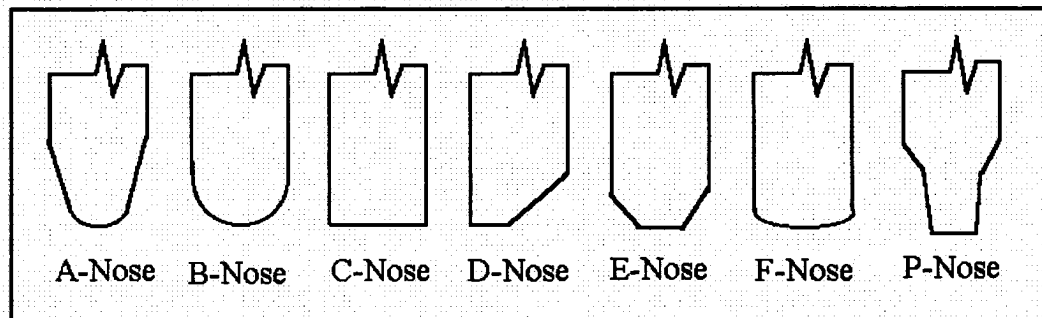


Figure 5: Standard electrode geometries [7]

2.3 Laboratory Test Methods

There are several laboratory tests available for evaluating electrode performance. *Electrode life* can be defined as the number of welds a pair of electrodes is able to produce during a repeatable application while maintaining a specified minimum weld size [1, 8]. Electrode life is evaluated through laboratory testing and is used to estimate electrode feasibility in a production environment.

The two most common ways to evaluate electrode life in the laboratory are the American Welding Society (AWS) D8.9 endurance test [9] and the General Motors (GM) WS-5A stepper test [10]. The oscillating weldability lobe test and sequential life test have also been employed to assess detailed aspects of electrode life.

2.3.1 AWS Endurance Test

The AWS endurance test evaluates electrode life by determining the number of acceptable welds that can be produced by a single pair of electrodes under constant current conditions. The acceptability criterion used is the minimum *weld button* size, which is given by the formula $4\sqrt{t}$, where t is the average sheet thickness in millimetres. A weld button is simply the weld metal, including all or part of the nugget, which remains after destructive testing is completed.

A weld size stabilization procedure is conducted prior to the beginning of the test to condition the electrode faces and promote reproducibility of test results. The stabilization procedure consists of adjusting the weld current as required to maintain a specified weld size. At the end of the stabilization period, which is never more than 250 welds, the minimum button and expulsion currents are determined. The operating current is set 200 amperes below the expulsion limit and is kept constant throughout the endurance test [9].

Five button size measurements are conducted from peel-test samples every 200 welds. The peel-test sample consists of two coupons, 1.5 x 4 inches (38.1 x 101.6 mm) each, which are welded to create two buttons about 1.5 inches (38.1 mm) apart. The sample is peeled apart and the diameter of the second weld is measured with a micrometer, as shown in Figure 6. The test is terminated when the button size of all five peel-test samples are below the minimum button size for two consecutive 200-weld checkpoints.

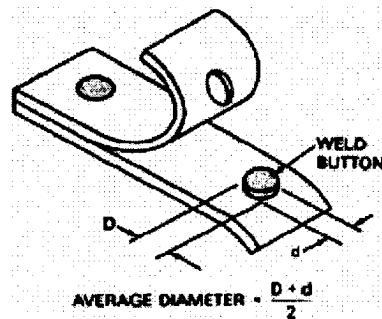


Figure 6: Measuring button size from a peel-test sample [11]

2.3.2 GM Stepper Test

The GM stepper test procedure is used to determine electrode life relative to other electrodes for a particular welding application. The test is also used to determine electrode life associated with a certain material and or sheet steel stack-up. The test involves increasing the weld current once the weld button size falls below a minimum specified value.

The weld button size is determined from a peel-test sample, as shown in Figure 6, every 100 welds. If the button size does not meet the minimum requirements at the 100-weld interval check, the current is increased in 100 ampere increments until the minimum size is reached. An additional 500 amperes is added to this current level and welding is continued.

There are several termination criteria for the GM stepper test. The test is continued until one or more of the following conditions occur [10]:

- a) the electrode cap sticks to the sheet;
- b) minimum button size can no longer be obtained with weld current increases;
- c) the weld current exceeds a specific, limiting current level;
- d) the electrode face diameter of either electrode exceeds a specified maximum.

2.3.3 Oscillating Weldability Lobe Test

The oscillating weldability lobe test measures the current range over the life of the electrodes. This is determined by measuring the nominal and expulsion currents as a function of the number of welds. The test is essentially an electrode life test during which the welding current is periodically oscillated between nominal and expulsion conditions [12, 13]. Electrode performance in this test is gauged on the consistency of the slope of the nominal and expulsion current lines. This test gives the user information about the current range at any point during electrode life. The data from this test may be more useful in a production environment where process reliability is a major concern.

2.3.4 Sequential Life Test

The sequential life test has been performed on zinc-coated steels [14-18] to gain insight into the development of electrode wear. Typically the test is run at constant

current with the electrodes being removed at pre-determined weld numbers. Characterization techniques include measuring the thickness of the brass-alloy layers at the electrode face, determining alloy layer composition, and hardness mapping. However, the costs involved in sequential life testing can be prohibitive making its application limited [17].

2.4 Production Welding

Electrode life tests provide a comparative measure of how electrodes perform under highly controlled conditions. Laboratory tests are not intended to simulate production welding conditions or estimate electrode performance in production operations [9]; as such the results are not directly transferable to the production environment.

2.4.1 Production-Specific Issues

Certain production-specific issues are not encountered in a laboratory test setting. These production-specific issues include increased operating current, equipment maintenance, factory personnel, and weld schedule compromise.

Production welding operations are often performed at much higher current levels when compared to laboratory tests. These higher currents seem to compensate for inconsistencies in materials, prior processing, welding equipment and other adverse production conditions. Natale [19] has noted that consistent weld quality in production is promoted by welding with a slight amount of interfacial expulsion in conjunction with application-specific weld schedules. Karagoulis [20] also found that the weld process itself behaves more robustly when it is tuned to operate at the expulsion limit. However, welding above the expulsion current level leads to accelerated electrode wear rates [21].

Equipment maintenance has been cited as a leading cause of discrepant weld quality in an automotive plant [20]. The study concluded that the key maintenance variables were secondary loop resistance, water flow, mechanical gun condition, and welding current. When preventive maintenance and improved process monitoring were introduced to production welding guns, perfect weld quality was achieved during several extended production runs.

Factory personnel also have an effect on the efficiency and reliability of the welding process. Standard weld parameters may be adjusted to satisfy the personal preferences of the welding engineers and technicians. Well-trained and competent factory personnel are better able to address and correct welding problems by having a more fundamental knowledge of the resistance spot welding process.

Weld schedules are often a compromise between productivity and electrode life. Electrodes in an automotive assembly plant are normally replaced at convenient times such as during breaks, lunches, or shift changes. Since the electrodes in a given area are replaced at the same time, electrode life is based on the worst-case electrode pair. Furthermore, production fluctuations require that the electrodes be able to extend to a maximum number of welds. Therefore, some electrode life remains unused for the sake of productivity.

2.4.2 Methods to Extend Electrode Life in Production

Repeated welding leads to thermal degradation of the electrode, which is manifested by an increase in the electrode face diameter. The current density drops and weld size is decreased, sometimes even to the point of not making a weld. A short electrode life can limit the rate of production that can be achieved in a fixed period of time by requiring frequent replacement of electrodes. The two methods of extending electrode life in production are *current stepping* and electrode dressing.

Current stepping is a process whereby the weld current is systemically increased to accommodate for electrode face enlargement and maintain current density. When stepping occurs too frequently, the electrodes are exposed to higher than necessary welding current and electrode deterioration is increased. When stepping does not compensate for the increase in face diameter, undersized welds are produced. Stepping the current ceases when the current capacity of the welding transformer is approached, or when further increases in current no longer produce acceptable welds.

Electrode dressing is a process whereby the electrode face is reconditioned with a tool to restore the initial face diameter. The dressing tool removes material only from the periphery of the face so as not to destroy the equilibrium established between the electrode and work material. The dressing frequency depends on the severity of the

welding environment. Dressing is terminated once the electrode face thickness falls below a minimum value. When this distance becomes too short, overheating of the electrode can occur.

The choice to employ stepping, dressing, or a combination of the two is determined by a given company. The development of the actual stepping or dressing procedure is carried out by plant personnel in accordance with corporate standards.

2.5 Galvanized Steel in the Automotive Industry

Galvanized steels were adopted by the automotive industry for their improved corrosion resistance properties. The zinc coating acts as both a physical and sacrificial barrier to keep the corrosive environment away from the steel surface. Over the years, the use of galvanized steels has gradually escalated from underbody members with perforation corrosion to exterior panels where cosmetic corrosion occurs [22].

2.5.1 Types of Galvanized Coatings

The automotive industry uses a wide variety of galvanized coatings; each engineered with specific properties. Three of the most common galvanized coatings used in the automotive industry are hot-dipped galvanized (HDG), galvanized (GA), and electrogalvanized (EG).

A hot-dipped galvanized coating is produced on a steel substrate by immersing it in a bath of molten zinc. Upon emergence from the bath, the thickness of the coating is controlled by the air-knives method and then allowed to solidify [22]. Table 2 indicates the iron-zinc alloys that are present in a typical hot-dipped galvanized coating. The ratio of the total thickness of the alloy layers to that of the outer free-zinc layer is affected by the bath immersion time [23]. Longer immersion times provide more time for diffusion and result in thicker iron-zinc alloy layers. The iron-zinc alloy portion of the coating usually represents 50 to 60 percent of the total coating thickness; the surface remains primarily unalloyed free zinc [23]. Aluminum is added to suppress the formation of alloy layers and to improve the adhesion between the coating and the steel substrate [23, 24].

Layer	wt% Zn
Zinc	100
Zeta (ζ), FeZn ₁₃	94
Delta (δ), FeZn ₁₀	90
Gamma (Γ_1), Fe ₅ Zn ₂₁	75
Base Steel	0

Table 2: Iron-zinc alloy compositions in a hot-dipped galvanized coating [23, 25]

A galvanized coating is produced by heating a hot-dipped galvanized sheet in a furnace at approximately 550°C [24]. All of the free zinc is converted to iron-zinc alloy producing a coating with a spangle-free surface finish and a dull grey appearance. The two primary reasons for the use of galvanized coatings are improved spot-weldability and enhanced paintability [23, 24].

Zinc can also be electrodeposited on the base steel to produce a thin uniform coating of pure zinc. Electroplating is done in a continuous plating cell, in which the moving annealed strip becomes the cathode in a flowing electrolyte bath [22]. Electroplated coatings have excellent adherence, a homogeneous structure, and a fine spangle-free surface finish [23].

2.5.2 Resistance Spot Welding of Galvanized Steel

When welding uncoated steel, nuggets form at the faying interface despite gross electrode face enlargement because of the heat generated from the high hardness, and hence high interfacial resistance, of the sheet surfaces. The surface resistance restricts the spread of current to the high contact pressure locations thereby maintaining an adequate current density [1]. Gould and Peterson [26] found that button size and the position of the current range were nearly invariable throughout electrode life when welding uncoated steel. Failure to form a weld nugget is attributed to an increased rate of heat conduction away from the faying interface, lowering the current density below the minimum required to produce a weld [27]. Electrode life values of 50,000 welds have been noted when welding uncoated steels [1].

Galvanized coatings are much softer and more conductive than the steels to which they are applied. The soft asperities on the galvanized coatings deform easily under pressure, resulting in a very low resistance that spreads the current over a large effective contact area. Thus, the effect of gross electrode face enlargement is far more detrimental to weld initiation and growth than for uncoated steels [1].

High speed photography was used to demonstrate that longer weld times are required to spot weld galvanized steel. This increase is necessary to melt and displace the zinc coating from the weld zone during the first few cycles [27]. Similar to uncoated steel, the remaining cycles are used for initiation and growth of the weld nugget.

Higher welding currents are required when welding galvanized steels to overcome the reduced heat generation at the faying interface. Howe [28] notes that the displaced zinc at the faying interface forms an annulus around the periphery of the weld through which a portion of the weld current is shunted. The initial delay required for zinc displacement leaves less time for the formation of the weld, thus necessitating higher weld currents. Since galvanized steel has a lower contact resistance than uncoated steel, less heat is generated at the electrode-sheet interface and heat conduction away from the weld zone is more rapid [29]. Clearly the ability to generate heat at the faying interface is reduced while the tendency to lose heat to the electrodes is increased.

2.5.3 Galvanized Steel and Electrode Life

Electrode life when resistance spot welding galvanized steel is significantly shorter than for uncoated steels. The steel substrate, type of galvanized coating, and surface finish all have an effect on electrode life.

Since harder steel substrates have higher bulk resistance, electrode life generally improves as the strength of the steel substrate increases. Steel substrates that are more resistive have increased bulk resistance, which increases heat generation in the steel and requires lower welding currents.

Zinc-alloy coatings, such as galvanized, tend to have longer electrode lives than free-zinc coatings due to increased coating hardness and resistivity. The increased hardness and resistivity result in higher faying interface resistance, which promotes weld initiation and lower current requirements compared to free-zinc coatings [30].

Surface finish can also have an effect on electrode life by altering the contact resistance of the workpieces. In general, surface treatments that increase contact resistance require less current and result in increased electrode life. Rough surface finishes, such as regular spangle, introduce variability to the process due to the deviation in roughness from point to point.

2.5.3.1 Hot-Dipped Galvanized Coatings and Electrode Life

Peterson [1] has noted that the electrode life of hot-dipped galvanized coatings is considered the worst-case scenario and is commonly the baseline by which all coated steels are measured. The free-zinc coating results in a low interfacial resistance and higher current requirements.

Increased aluminum content in the coating has been associated with reduced electrode life [14, 15, 31]. It was originally thought that the accumulation of a highly resistive aluminum oxide on the electrode face led to increased heat generation [14, 15]. However, it has been shown that sheets with higher aluminum contents form a Fe_2Al_5 inhibiting layer at the substrate-coating interface [31, 32]. This inhibiting layer acts as a barrier to the formation of iron-zinc alloys, and lowers the melting point of the coating. This phenomenon accelerates electrode wear through increased alloying between the electrode and the coating, resulting in shorter electrode life [31].

2.5.3.2 Galvannealed Coatings and Electrode Life

Galvannealed coatings produce longer electrode lives when compared to hot-dipped galvanized coatings [19, 33]. The increased hardness of galvannealed coatings over hot-dipped galvanized coatings, attributed to the formation of iron-zinc intermetallics, allows them to be resistance welded with lower weld currents.

The iron in the galvannealed coating leads to a very prominent FeZn parting layer on the electrode face. Lu et al. [16] have noted that this parting layer increases electrode life by acting as a barrier to the underlying brass phases. Pickett et al. [34] found that electrode life improved as the total iron content of the coating increased. It was also determined that the optimum material for weldability consists of a thin discontinuous

gamma phase at the steel interface and an intermittent zeta phase on the surface of the coating.

2.6 Electrode Wear Mechanisms for Galvanized Steel

The high temperatures and pressures encountered in the resistance spot welding process expose the electrodes to both thermal and mechanical stresses. These stresses cause the strengthening mechanisms of the electrode material to deteriorate. When resistance spot welding galvanized steel, the copper-based electrodes also alloy with the zinc coating. This alloying causes undesirable changes in the electrical, thermal, and mechanical properties of the electrode material.

The composition of the electrode material, electrode geometry, steel substrate, coating type, and weld schedule all influence the extent of electrode wear. The electrode wear mechanisms for galvanized steel include: brass-alloy formation on the electrode face, mushrooming, sticking and brassing, pitting and cavitation, and cracking. One beneficial reaction that can occur on the electrode face is the formation of a protrusion.

2.6.1 Brass-Alloy Formation on the Electrode Face

Temperatures at the electrode-sheet interface are high enough to allow atomic diffusion between zinc and copper. The transfer of zinc atoms at the electrode-sheet interface results in the formation of brass-alloy layers on the face of the electrode. The extent of zinc diffusion depends on the time-temperature history of the interface, the characteristics of the galvanized coating, and electrode composition.

The surfaces of new electrodes experience a rapid transformation during their first few welds. Well defined brass-alloy layer boundaries have been noted on the electrode face as early as five welds into electrode life [35]. The brasses that form on the face of the electrode have lower electrical and thermal conductivities than the copper-based electrode material, resulting in higher temperatures at the electrode-sheet interface. As well, they have lower melting temperatures and generally lower strength. The increase in homologous temperature (T/T_m) that results from higher operating and lower melting

temperatures combined with the decreased strength of the brass-alloys causes faster deformation rates at the electrode face.

The chemical compositions of the brass-alloy layers are well correlated with the compositions given by the Cu-Zn phase diagram, as shown in Figure 7. The outermost phase on the face of the electrode is a porous dark-grey iron rich parting layer, followed by a white gamma-brass layer, and a yellow beta-brass layer. The innermost layer corresponds to alpha-brass, which is usually very thin and difficult to distinguish from the base copper. The complete absence of the alpha-brass phase has been noted [7, 17]. Howes and Lake [35] have shown that there is no difference in the composition of an alloy layer with increasing weld number.

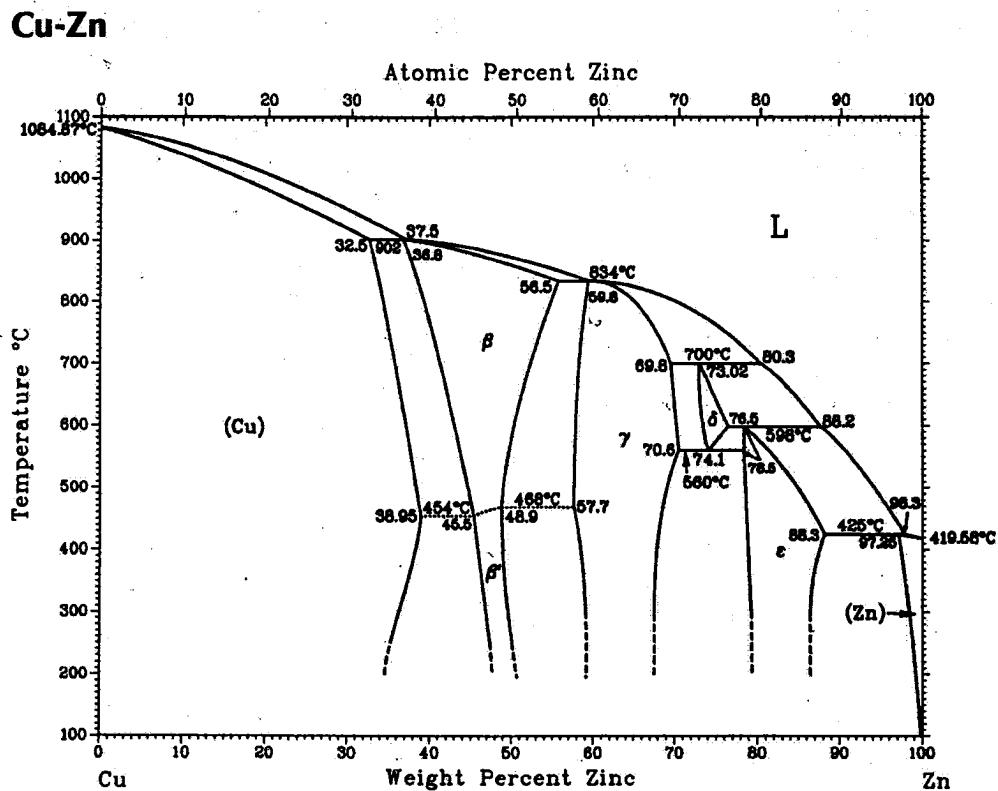


Figure 7: The copper-zinc phase diagram [36]

2.6.2 Electrode Face Enlargement

Electrode face enlargement, commonly referred to as mushrooming, occurs as material from the electrode face is extruded to the periphery causing an increase in the electrode face diameter. The two types of mushrooming that have been observed are brass-alloy extrusion and bulk copper extrusion.

2.6.2.1 Brass-Alloy Extrusion

The extrusion of brass-alloys occurs early in electrode life and can exist without bulk copper extrusion. Dong and Kimchi [37] believed this extrusion to be a consequence of the decrease in the beta-brass flow stress at high temperatures coupled with the thermal gradient that develops between the electrode body and face during the hold time. Since the electrode cools from the water channel outward, the face remains at a higher temperature than the body upon cooling. It is proposed that the electrode body contracts independently of the electrode face along the beta-brass interface. The high temperature, low strength beta-brass accommodates this contraction by extrusion. Finite-element modelling confirmed that the overall brass extrusion results from an accumulation of these incremental extrusions [37].

2.6.2.2 Bulk Copper Extrusion

Extrusion of bulk copper has been noted to occur in the middle to late stages of electrode wear after brass-alloy extrusion has taken place [14, 15]. Thermal degradation of the strengthening mechanisms of the bulk electrode material causes significant softening and gross extrusion. The extrusion process is the same as that proposed for brass-alloy extrusion. Gross deformation could also be the result of a thermal fatigue or creep-type mechanism [38]. A combination of these phenomena may exist concurrently and extend to different depths below the electrode face.

2.6.3 Sticking and Brassing

Electrode sticking is the bonding of the interface between the galvanized coating and the brass-alloys on the electrode face. One cause of sticking is attributed to liquated brass penetrating into the grain boundaries of the galvanized steel. Sticking is most often

encountered early in electrode life and is usually not a factor once the brass layers on the electrode face have stabilized [39]. In certain cases, sticking is so severe that the electrodes can be pulled from their holders.

Irving [6] notes that DSC electrodes have reduced sticking frequency when compared to CuZr or CuCr electrodes. It has been suggested that the aluminum oxide on the electrode surface inhibits wetting of the molten zinc and brass [1]. Conversely, CuCr electrodes exhibit the most severe sticking behaviour in terms of frequency and strength of sticking [39, 40].

Sticking may lead to brassing, where layers of brass are removed from the electrode face and deposited on the galvanized steel surface. This deposition usually results in a visually undesirable surface. The random transfer of yellow beta-brass onto the steel surface may be aided by cracks along the gamma-beta interface [41]. Gallagher et al. [18] have pointed to the transfer of gamma-brass, its white colour making it less visually detectable than yellow beta-brass, as a possible primary mechanism of electrode erosion.

2.6.4 Pitting and Cavitation

Pitting is a common aspect of electrode wear and has been noted on the electrode face on several occasions [15, 39, 42, 43]. Pits can form after a single weld event, and either agglomerate together to form larger pits or disappear after additional welds. Gugel et al. [15] noted that a healing process occurs whereby the continued forging action during welding results in metal flow that fills in smaller pits.

For welding currents below expulsion, studies have shown that CuCr and CuZr electrodes tend to form small pits that coalesce into a large central pit while DSC electrodes tend to form pits that do not coalesce [39, 42]. When welding currents are above the expulsion limit, central pitting is common for all electrode materials [1]. Gugel et al. [42] noted that at higher current levels, DSC materials have the ability to self-heal, whereas CuCr and CuZr electrodes have softened too much and wear rapidly. The superior performance of DSC electrodes in current stepping tests is best explained from this observation.

Pitting has been reported to affect the shape of the weld nugget by inhibiting local current flow. It is believed that a non-uniform current density results from the current being forced to use the remaining contact surface. Hot spots are created on the electrode face accelerating thermal damage, causing irregular nugget penetration and weld button size variation [15, 37]. Wist and White [39] noted that the fracture or shear of the brass-alloy layer may play a critical role in the pitting process by bringing the zinc rich phases into closer contact with the underlying electrode material.

Cavitation is the formation of a central pit spanning a considerable amount of the electrode face. Concentrated thermal damage about the central portion of the electrode face may result in the coalescence of smaller pits to form a cavitation. Cavitation often results in the end of electrode life.

2.6.5 Cracking

Peterson [1] notes that cracking of the electrode face most likely occurs from thermal-expansion-induced residual stresses. Cracks form because the state of stress at the electrode face, and the high-temperature strength of the electrode material do not allow relaxation to be accommodated by mushrooming.

Cracks are usually oriented radially from the centre of the electrode face and cause the current distribution to be segmented in much the same way as pits. Cracking is common in DSC materials since thermal stresses are generated from differences in the thermal expansion of copper and the dispersoids.

2.6.6 Protrusions

A protrusion is the build up of brass or galvanized coating that extends beyond the central portion of the electrode face. Protrusions may also result from annular wear along the electrode face periphery.

The presence of a protrusion has been reported to be beneficial for electrode life when welding galvanized steels [16, 34]. The protrusions may extend electrode life by reducing the effective contact area, increasing the current density and stabilizing nugget formation. The protrusion may also act as a zinc diffusion barrier by forming a wear

layer that thermally isolates the electrode body from increased levels of thermal degradation.

2.6.7 Electrode Wear Sequence

In the beginning stages of electrode wear, the electrode face goes through a substantial metallurgical transition. The rapid diffusion of zinc creates a series of brass alloys on the electrode face. Sticking between the electrode and sheet is pronounced, leading to the deposition of brass onto the galvanized sheet. The stage culminates in the formation of a stable set of brass alloys on the electrode face.

The middle stage of electrode wear begins with geometric changes on the electrode face. The most notable change is the extrusion of brass-alloy layers to the periphery of the electrode face. Cracking, pitting and the formation of protrusions also begin during this stage.

The final stage of electrode wear is characterized by extrusion of the bulk copper material from the electrode face. This occurs after thermal softening has defeated the strengthening mechanisms of the bulk copper. Pit consolidation also occurs in the final stage, often focusing on the central portion of the electrode face.

III. EXPERIMENTAL MATERIALS AND PROCEDURE

The performance of two developmental electrodes was evaluated through both laboratory and production testing. The GM WS-5A stepper test [8] was carried out at the General Motors Technical Center in Warren, Michigan. Electrode life was determined on hot-dipped galvanized steel. The DaimlerChrysler (DCX) beta-site trials were performed at the Windsor Assembly Plant (WAP) in Windsor, Ontario. Electrode performance was evaluated on galvanized steel through adjustments to the weld schedule. In each case, the performance of the developmental electrodes was evaluated relative to the performance of a baseline electrode.

3.1 Electrode Properties

All of the electrodes tested during this investigation were female B-nose cap electrodes, as shown in Figure 8, with a 15.9 mm (5/8-inch) body diameter and 4.8 mm (0.188-inch) face diameter. The B-nose geometry was chosen to conform to existing production practices. The CuZr electrode is the baseline electrode for the GM stepper tests, as mandated by the test procedure. The WAP electrode represents the baseline electrode for the DCX beta-site trials; it was in use for the particular welder where the testing was conducted. The M and the FIN represent the developmental electrodes. The M electrode was manufactured from a proprietary oxide dispersion strengthened (ODS) copper. This material was chosen for its consistent performance in several previous laboratory tests. Copper-zirconium was chosen for the FIN electrode because of its high conductivity and proven performance in production. The composition and geometry alterations for each of the electrodes are provided in Table 3.

To enhance the cooling properties of the developmental electrodes, the face thickness was reduced to 6 and 7 mm, from a typical thickness of 10 mm, for the M and FIN electrodes respectively. Fins were also formed in the water channel of the FIN electrode to further enhance cooling. Attempts to cold-form internal fins on the M electrode resulted in cracking. A sectioned view of the FIN electrode is provided in Figure 9. The fins are triangular in shape and extend nearly half the depth of the water channel.

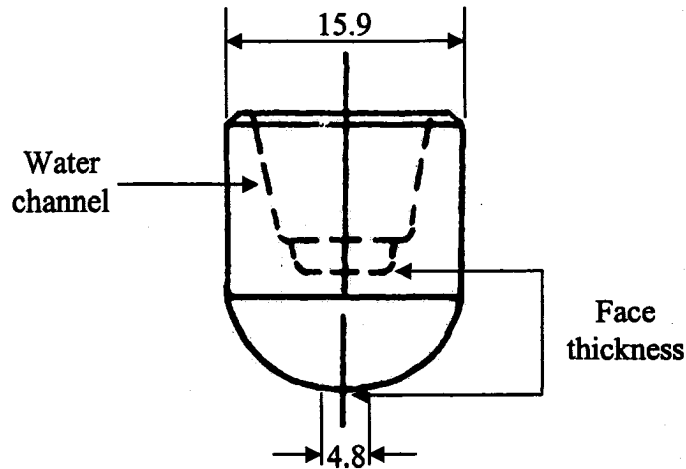


Figure 8: Female B-nose electrode cap used for the testing (dimensions in mm)

Electrode Name	Composition (Cu +)	Geometry Alterations
CuZr	0.15 wt% Zr	N/A
WAP	Body: 0.15 wt% Zr Insert: 1.1 wt% Al ₂ O ₃	N/A
M	1.1 wt% Al ₂ O ₃ + 0.15 wt% mixed oxides of Ti, Fe, and Si	6 mm face thickness
FIN	0.15 wt% Zr	7 mm face thickness + internal fins

Table 3: Composition and geometry alterations for each of the tested electrodes



Figure 9: Sectioned view of the FIN electrode showing the fins in the water channel. The fins are triangular in shape and extend nearly half the depth of the water channel.

3.2 GM Stepper Tests Procedure

The chemical composition, coating properties, and mechanical properties of the galvanized sheet steel used in the GM stepper tests are summarized in Table 4. The cold rolled high strength low alloy (HSLA) steel, with minimum yield strength of 350 MPa (50 ksi), was supplied by AK Steel Corporation. The steel substrate had an average thickness of 1.12 mm and was coated with a minimum spangle hot-dipped galvanized coating. Hot-dipped galvanized steel was selected because it represents the most severe condition with respect to electrode life.

The weld parameters for the GM stepper tests are listed in Table 5. The tests were conducted using a pedestal welder with an air-operated cylinder, Miyachi MM-326B current analyzer, and a digital read-out force gauge. The electrode force and weld time were set according to GM WS-4A as a function of sheet coating and thickness. The weld current required to obtain minimum button size (4.0 mm), as specified in GM4488M, was determined by welding peel-test samples. The current at the beginning of the test was set 500 amperes higher than the determined minimum button current.

Peel tests were conducted every 100 welds to determine if minimum button size had been maintained. If minimum button size was achieved, welding was continued at the same current level. If minimum button size was not achieved, the current was increased in 100 ampere increments until minimum button size was re-obtained. Once minimum button size was re-obtained, 500 amperes was added to the current level and welding continued. The GM stepper test was continued until one of the previously mentioned termination criteria (Section 2.3.2) was met.

Electrode alignment was determined from carbon imprints taken prior to the first weld, after 200 welds, after 500 welds and after every successive 500-weld interval. Carbon imprinting, as shown in Figure 10, involves the application of welding force, without the weld current, to a single coupon sandwiched between carbon paper and white paper. An impression of the electrode face is left on the white paper, revealing the shape of the contact surface between the electrode and work sheets. Carbon imprints are particularly useful in exhibiting any evidence of pitting on the electrode face.

Chemical Composition (wt%)							
C	Mn	P	S	Si	Cr	Ni	Mo
0.071	0.72	0.006	0.009	0.012	0.025	0.006	< 0.003
Cu	Al	Ti	Nb	V	B	Ca	N
0.018	0.047	< 0.003	0.018	< 0.003	< 0.003	< 0.003	0.0036

Coating Composition (wt%)				Coating Weight (g/m ²)		
Surface	Al	Fe	Pb	Edge X	Centre	Edge Y
Top	0.42	0.24	0.005	79	73	76
Bottom	0.44	0.20	0.005	82	82	82

Mechanical Properties						
Orientation	YPE (%)	Lower YS MPa (ksi)	UTS MPa (ksi)	Elongation (%)	n-Value	Hardness (HRB)
Longitudinal	1.5	374 (54.2)	469 (68.0)	29.8	0.164	76
Transverse	2.9	406 (58.9)	478 (69.4)	31.0	0.155	77

Table 4: Chemical composition, coating properties, and mechanical properties of the hot-dipped galvanized sheet steel used for the GM stepper tests

Weld Parameter	Value
Electrode Force	670 lbf (2.98 kN)
Squeeze Time	30 cycles
Weld Time	16 cycles
Hold Time	2 cycles
Weld Rate	30 WPM
Minimum Button Size	4.0 mm
Water Flow Rate	0.5 gpm (1.9 L/min)

Table 5: Weld parameters for the GM stepper tests

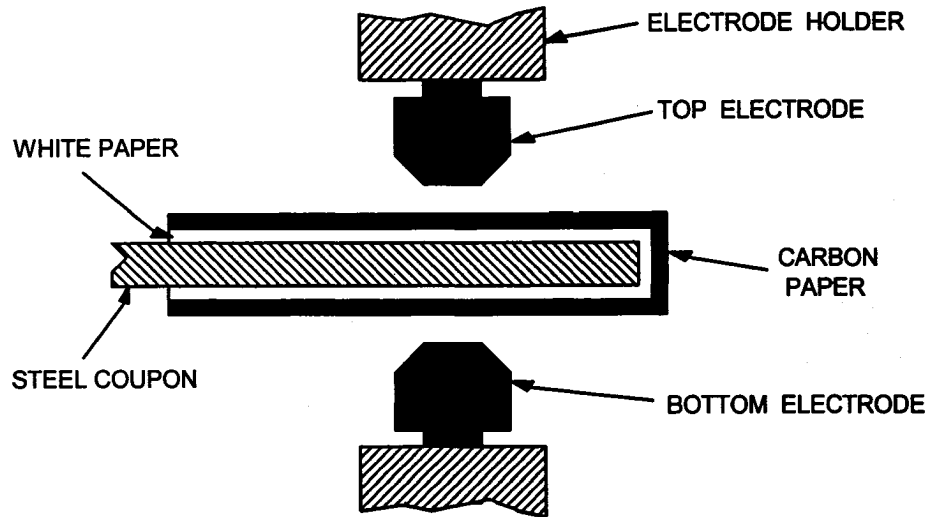


Figure 10: Carbon imprint schematic [9]

3.3 DCX Beta-Site Trials Procedure

The DCX beta-site trials used a programmed initial current and stepper schedule to weld a non-safety critical part. The application involved a two thickness stack-up, 1.21 mm to 0.71 mm, with a weldable sealer applied at the interface of the two parts. The assembly was robotically manipulated with 11 welds being performed in 18 seconds. The minimum cycle time for welding and part manipulation was 45 seconds. The average cycle time allowing for intermittent production stoppages was approximately 1 assembly per minute. The weld parameters are outlined in Table 6.

The minimum allowable button size for the application was 3.1 mm as given in DCX Process Standard 9471 (PS-9471) [44]. During the testing, periodic button size measurements and weld quality inspections were performed through destructive peel tests, chisel checks, and ultrasonic testing.

A current range test was conducted for each electrode to determine an appropriate starting current. The beginning current in the current range test was set at 6500 A and increased in 250 A increments until the first instance of expulsion occurred. The expulsion current was used as a reference in determining an appropriate starting current for the trials. The term expulsion is used to represent interfacial expulsion as opposed to surface expulsion. Interfacial expulsion refers to the expulsion of metal from between the

sheets, where the weld nugget is being formed. Surface expulsion occurs at the electrode-sheet interface and can occur when the sheet surface contains oil or grease.

Weld Parameter	Value
Electrode Force	380 lbf (1.70 kN)
Squeeze Time	30 cycles
Weld Time	10 cycles
Hold Time	2-4 cycles
Weld Rate	11 welds / 18 seconds
Minimum Button Size	3.1 mm
Water Flow Rate	4.0 gpm (15.1 L/min) average

Table 6: Weld parameters for the DCX beta-site trials

The visual detection and counting of interfacial expulsions was employed to provide a benchmark for electrode performance. The number of expulsions per assembly was counted and recorded through Passive Data Collection (PDC). The data collection is termed passive because there are no engineering adjustments to the process beyond those adjustments that are part of a normal production operation [45]. The number of expulsions per assembly provided a reference to the weld lobe as welding progressed. A voting technique among the project members was employed to determine the number of welds per assembly that displayed expulsion. Expulsion was easily detected in most cases; as such, there was general concurrence by the project members.

Expulsion graphs depicting expulsions per assembly vs. assembly number were constructed. The expulsions per assembly were represented by a moving average of five assemblies. The moving average was selected to depict overall expulsion behaviour and eliminate graph sharpness. The moving average also represents a more conservative checkpoint of 55 welds compared to the 100-weld interval for the GM stepper test.

The development of a suitable weld schedule was achieved through adjustments to both the starting weld current and stepper rate. The goal was to reduce the current level, represented by the start current and stepper rate, to the lowest feasible yet reliable rate. Expulsion observations determined the direction of current level adjustment. The ability to maintain moderate expulsion, while preserving weld quality, was the main

determinant of stepper schedule feasibility. A prolonged period of several assemblies without any instances of expulsion resulted in the trial being terminated.

The starting current for the first trial was selected at least 250 A higher than the expulsion current from the current range test. For the preliminary trials, conservative stepper rates were employed to ensure weld quality and were lowered according to expulsion observations. Following acceptable expulsion observations with a constant stepper rate, the stepper schedule was adjusted in stages. The final adjusted stepper schedule increased the stepper rate for each successive stage to better maintain current density. Upon successful results from the preliminary trials, multiple production trials were carried out with the developed weld schedule to ensure process repeatability.

3.4 Metallographic Procedure

Upon completion of testing, the surface of the electrode face was documented via digital imaging at Inspect-X Testing Services in Windsor, Ontario. The magnification level was variable depending on the size of the face and was dictated by obtaining maximum screen fill. The electrode face diameters were measured using an Optical Gauging Products Smartscope MVP. The electrode face diameters were measured on the digital images by using a circle target which produced a best-fit result.

The top electrodes were sectioned on a Buehler Isomet 1000 saw with a 6-inch diameter diamond wafer blade set to a speed of 200 rpm. Varsol was used as a lubricant for the blade during cutting. The electrodes were first sectioned longitudinally at an offset to the centre of the face. The offset ensured that after grinding and polishing, the sample would provide a central profile of the electrode face. A second cut was conducted across the electrode body to produce two cross sections, as shown in Figure 11(a).

The electrode cross sections were mounted in a Buehler Simplimet 3 Mounting Press using blue Buehler Mineral Filled Diallyl Phthalate powder. The electrode cross sections were mounted at 150°C and 3000 psi for 2.5 minutes with no pre-load. Following mounting, identification labels were inscribed on the back of the 1.5 inch diameter samples. The sample edges were beveled on a Buehler Surfmet I Belt Surfacer silicon carbide belt grinder for easier handling in subsequent steps.

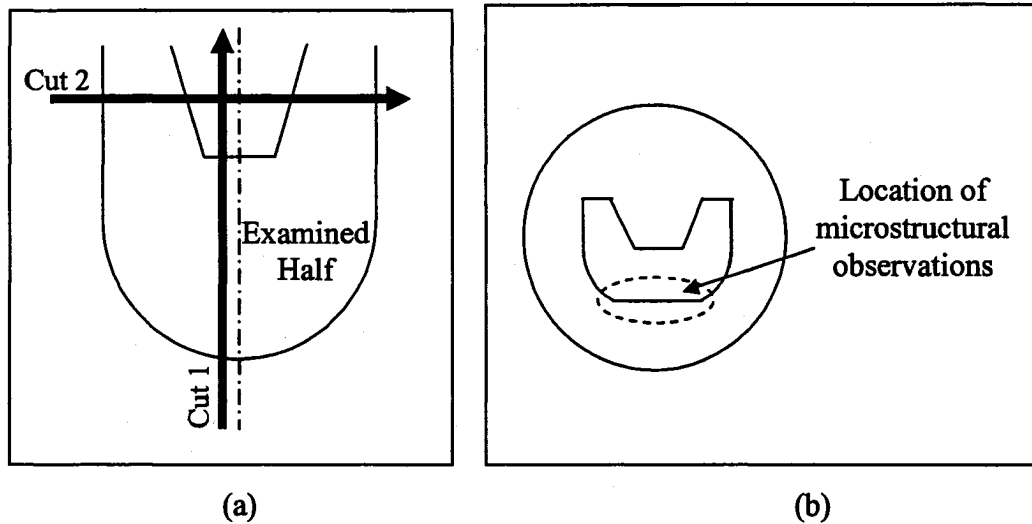


Figure 11: (a) Electrode sectioning schematic and (b) final mount sample showing the location of the microstructural observations

A Buehler Handimet II Roll Grinder was employed to rough grind the samples progressively through 240, 320, 400, and 600 grit silicon carbide papers. The samples were rinsed with soap and water and rotated 90 degrees between grits.

Initial polishing was accomplished on a Buehler Ecomet 3 Variable Speed Grinder-Polisher. The samples were polished using 9 μm diamond paste applied to a billiard cloth on a 9-inch diameter wheel. The speed of the wheel was set to 200 rpm. The main purpose of this step was to ensure that the sample was flat before fine polishing.

Fine polishing was accomplished on a Buehler Metaserv Grind-Polisher. The samples were polished using 1.0 μm Buehler Micropolish II Deagglomerated Alpha Alumina suspended in water. The aluminum oxide powder was applied to the billiard cloth on a 9-inch diameter wheel set to a speed of 200 rpm. Fine polishing was accomplished with 0.05 μm Buehler Micropolish II Deagglomerated Alpha Alumina oxide powder. The aluminum oxide powder was applied to the billiard cloth on a 9-inch diameter wheel set to a speed of 175 rpm.

Optical examination of the polished samples revealed the electrode face to consist of a dark grey surface layer, a white brass layer, and a yellow brass layer. The polished samples were etched with a solution of 5 g ferric chloride (FeCl_3), 2 ml hydrochloric acid

(HCl), and 100 ml ethanol to reveal recrystallization at the electrode face. Immediately after etching, the samples were briefly rinsed in cold tap water.

3.5 Alloy Layer Thickness Measurements

Alloy layer thickness measurements were conducted with a Buehler Omnimet Image Analysis System (Version 5.20) on samples polished through 1.0 μm aluminum oxide. Thicknesses were measured perpendicular to the electrode face at 500x magnification. The measurements were taken across the face of the electrode cross-section every 250 to 300 μm . Pitted areas as well as mushroomed areas at the edges of the face were not included in the measurements.

The composition of the individual layers was not determined since previous research confirmed that the yellow layer has a zinc composition corresponding to beta-brass and the white layer has a zinc composition corresponding to gamma-brass [17].

3.6 Hardness Measurements

To determine the depth of softening into the electrode face, Vickers microhardness testing was performed on a Buehler Micromet II Microhardness Tester using a 200 g load and an indentation time of 12 seconds. Hardness profiles into the electrode body were taken on the polished electrode cross-section beginning at both the centre and edge of the electrode face. Measurements were conducted every 0.1 mm for the first 2 mm of depth and every 1 mm thereafter.

IV. EXPERIMENTAL RESULTS

This chapter presents the results obtained from both the GM stepper tests and the DCX beta-site trials. The results from the GM stepper tests include the weld current and button size measurement graphs. The DCX beta-site trials results include the current range curves and expulsion graphs. Electrode face images and face diameter measurements are given for the tested electrodes. Microhardness results, alloy layer thickness measurements, and microstructural observations are also provided.

4.1 GM Stepper Tests Results

The weld current graphs for the CuZr, M, and FIN electrodes are shown in Figure 12. Each of the tests was terminated due to the maximum face diameter restriction of 10 mm. The CuZr achieved the longest life of 8500 welds, followed by the M at 7500 welds, and the FIN at 7000 welds.

Table 7 provides the line of best-fit equations and R^2 value for each of the electrodes. The intercept of the best-fit line, called the start current, represents the weld current once 500 amperes was added to the minimum button size current. The slope of the best-fit line, called the stepper, corresponds to the average current increase per weld necessary to maintain minimum button size. The R^2 value is an indication of how well the line of best-fit corresponds to the actual weld current data and thus gives a measure of the consistency of current increases.

The key evaluation criteria are the frequency, magnitude, and consistency of weld current increases. In terms of lowest final current and lowest stepper rate, the CuZr ranked first followed by the M and then the FIN. However, it is noted that the M demanded the lowest current levels for the first 5000 welds. The FIN provided the most consistent current increases as measured by the R^2 value.

Figures 13 to 15 show the button size measurements for each of the electrodes. A measurement of 0 mm corresponds to a no-weld condition. The baseline CuZr provided the most consistent button sizes and experienced only two no-weld dropouts. The M electrode produced six no-weld dropouts and displayed significant button size variability in the second half of the test; however, it did not produce its first no-weld until the 4300

weld checkpoint. The severity of the no-weld dropouts was most prevalent for the FIN electrode. Consecutive no-weld conditions were experienced on four occasions. At 5300 welds, eight peel tests were required, representing an increase of 800 A, to re-obtain minimum button size.

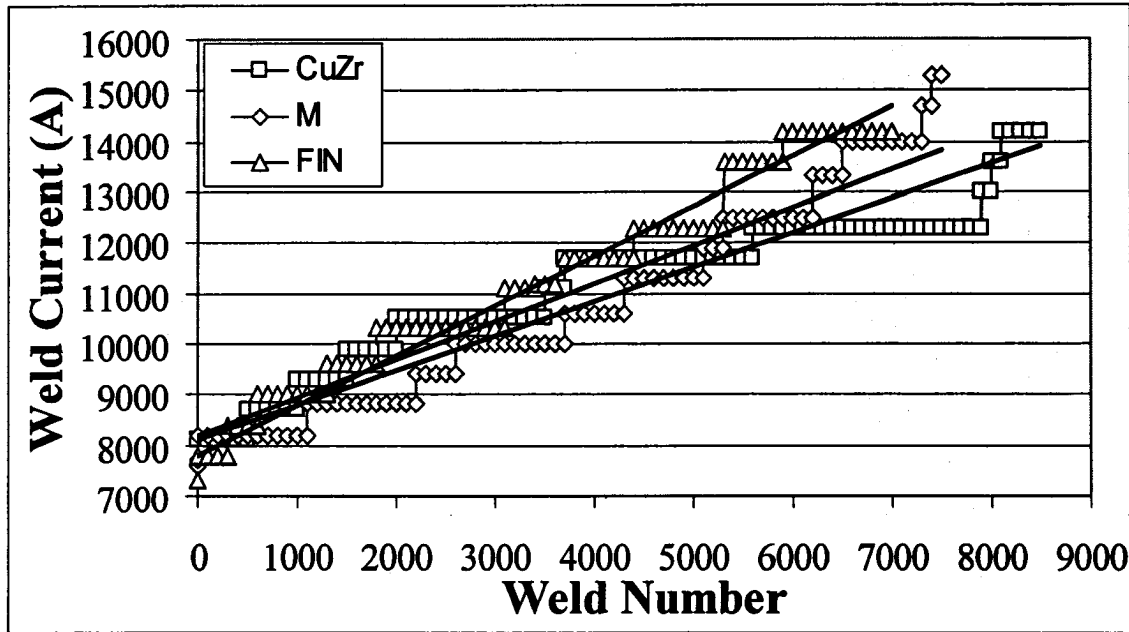


Figure 12: GM stepper tests results on hot-dipped galvanized steel showing the weld current vs. weld number data and line of best-fit for each electrode

Electrode	$Y = \text{start current (A)} + \text{stepper (A/weld)}$ $x = \text{number of welds}$	R^2
CuZr	$Y = 8100 + 0.69x$	0.8795
M	$Y = 8200 + 0.75x$	0.9187
FIN	$Y = 7800 + 0.99x$	0.9726

Table 7: Line of best-fit equations and R^2 values for the GM stepper tests

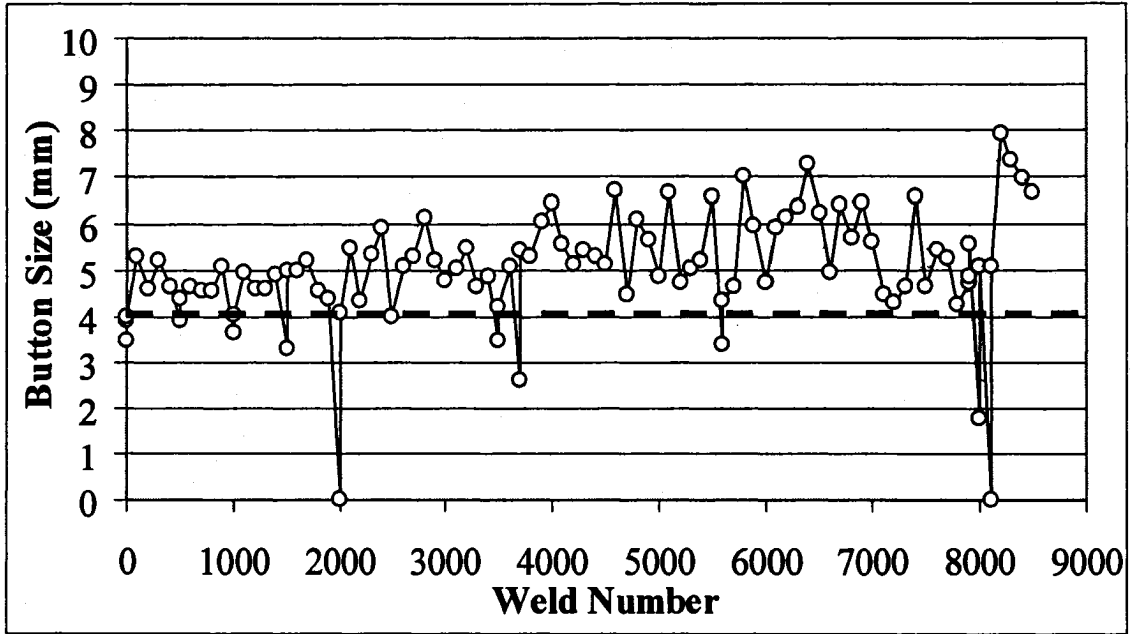


Figure 13: GM stepper test button size measurements for the CuZr electrode

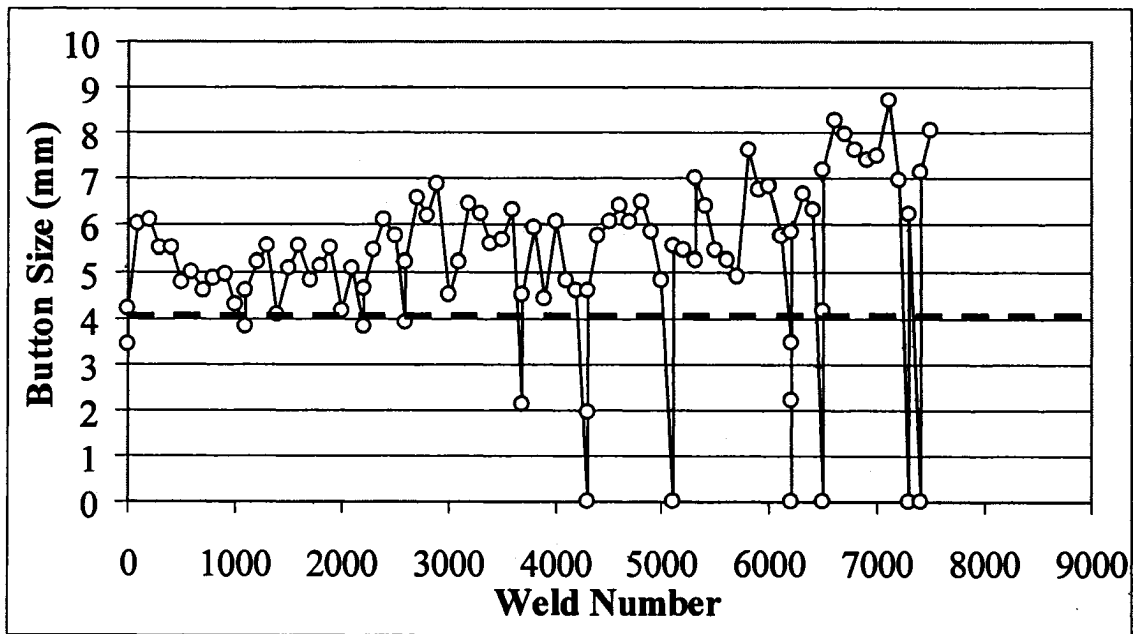


Figure 14: GM stepper test button size measurements for the M electrode

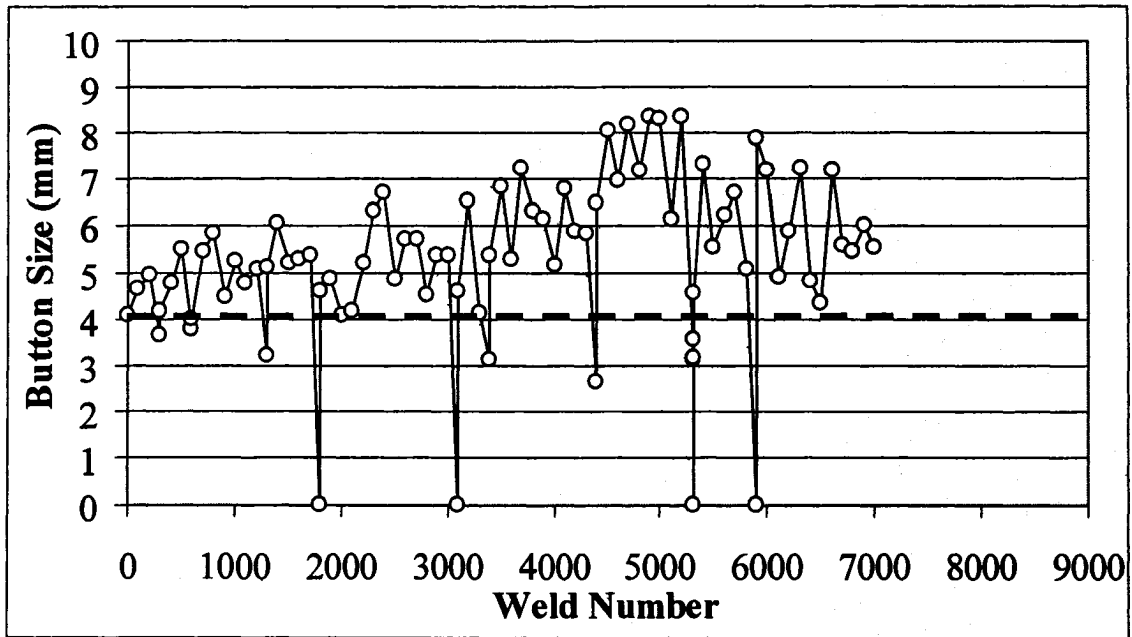


Figure 15: GM stepper test button size measurements for the FIN electrode

4.2 DCX Beta-Site Trials Results

The DCX beta-site trials represent the last step in qualifying the two prototype electrodes. The electrodes were required to show repeatable production welding performance in an automotive assembly plant.

Prior to the testing, electrode force was increased from 330 to 380 lbf and weld time decreased from 12 to 10 cycles as initial adjustments to the existing weld schedule. Both of these adjustments were made prior to the current range and in consultation with DaimlerChrysler Process Standard 9471 and American Welding Society Standard D8.9.

4.2.1 Current Range Results

The button size measurements for the current range test are shown in Figure 16. The expulsion current from the current range was used as a reference in determining an appropriate starting current. The first instance of interfacial expulsion was noted to occur at 7750 and 8250 A for the WAP and M electrodes respectively. For the FIN electrode, a very light expulsion, possibly surface expulsion, was observed at 8000 A with a more severe expulsion occurring at 8250 A. It is noted that each of these currents was below the starting current for the existing production weld schedule.

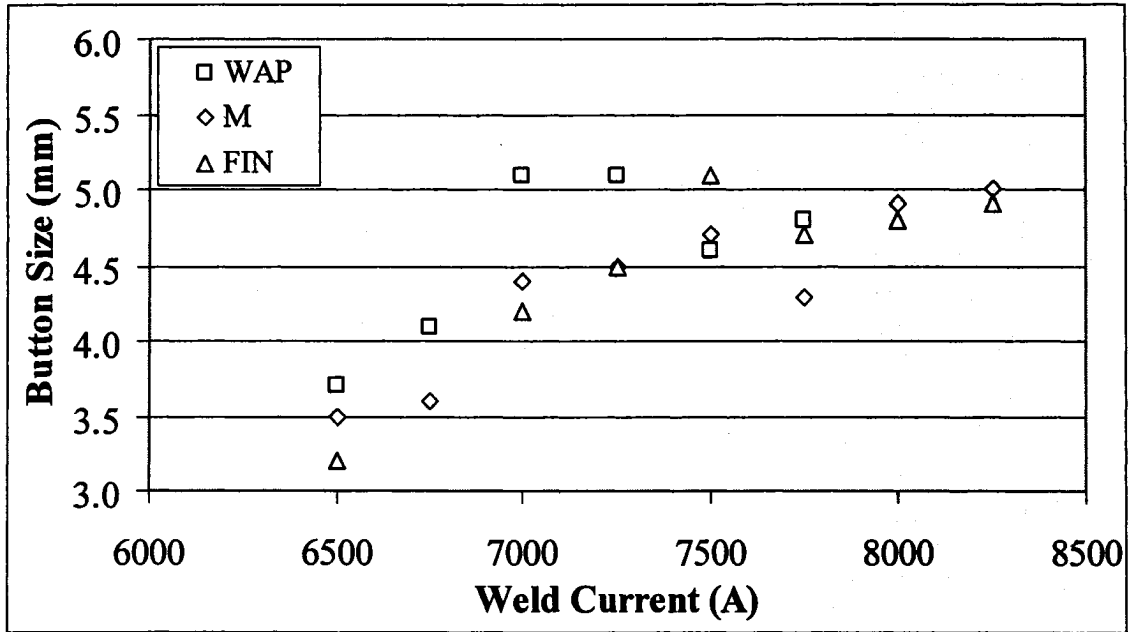


Figure 16: Button size measurements for the DCX beta-site trials current range test

4.2.2 Expulsion Observations - M Electrode

Figures 17 to 19 present the expulsion observations for the M electrode. Several abbreviated trials were initially conducted to determine the appropriate combination of starting current and stepper rate. The trials were terminated at different lengths due to electrode replacement feasibility. Decreases in starting current and stepper rate are shown to reduce expulsion frequency.

The weld schedule for the first trial consisted of a starting current of 8500 A and a conservative stepper rate of 2 A per weld. As expected, severe expulsion was experienced with these settings, as shown in Figure 17. For the second trial, the starting current was maintained at 8500 A while the stepper rate was lowered to 1 A per weld. These settings resulted in reduced expulsion frequency compared to the 2 A per weld stepper. The starting current and stepper rate were further adjusted downward for the following two trials. The lowest expulsion frequency was observed with a starting current of 8000 A and a stepper rate of 0.5 A per weld.

The trials with starting currents below 8500 A exhibited a running average below one expulsion within the first 125 assemblies. In order to increase the number of

expulsions while maintaining a reduced stepper schedule, an 8500 A starting current was selected in conjunction with a stepper rate of 0.75 A per weld. Two trials were conducted using these parameters. The expulsion graphs for the two trials, Figure 18, exhibit good correlation between 150 and 250 assemblies. In the second trial, the running average declined abruptly around 400 assemblies and remained low for the duration of the trial.

Based on an analysis of the results of the two trials, the mean stepper rate was adjusted to avoid the expulsion drop-off that occurred near the end of the second trial. To maintain current density in the final stage and limit initial thermal degradation of the electrode, the weld stepper was divided into three stages: 0.65 A per weld for the first 2500 welds, 0.75 A per weld for welds 2501-5000 and 0.85 A per weld for welds 5001-7500. In this way, the mean stepper rate was maintained at 0.75A per weld. Figure 19 displays the three 12-hour production trials carried out with the enhanced stepper schedule. The expulsion graphs display relatively consistent results with the running average decreasing gradually in the beginning stage, remaining moderate in the middle stage, and steadily increasing in the final stage. This provided evidence of the effectiveness of the weld schedule to maintain current density late in life.

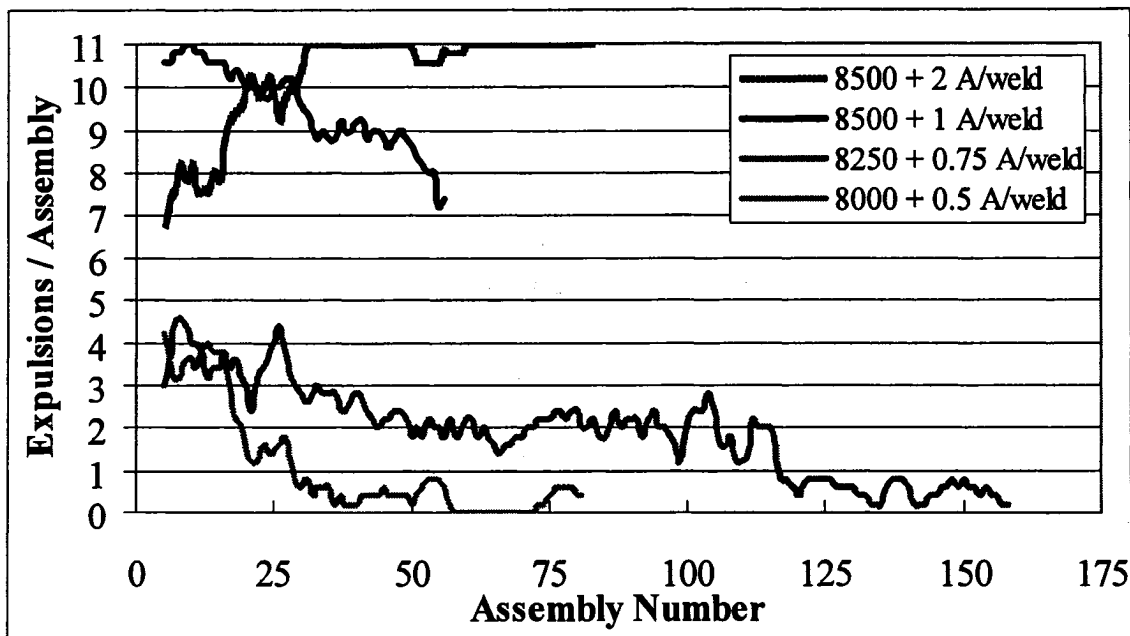


Figure 17: Expulsion observations for the preliminary M electrode trials

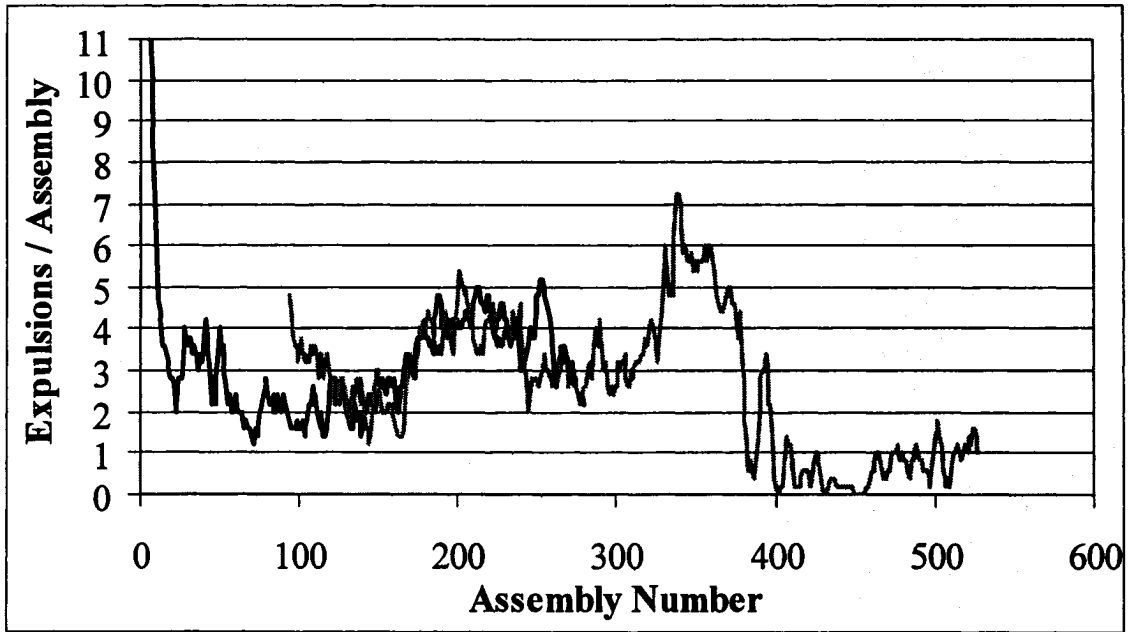


Figure 18: Expulsion observations for the M electrode trials conducted with an 8500 A start current and 0.75A per weld stepper rate

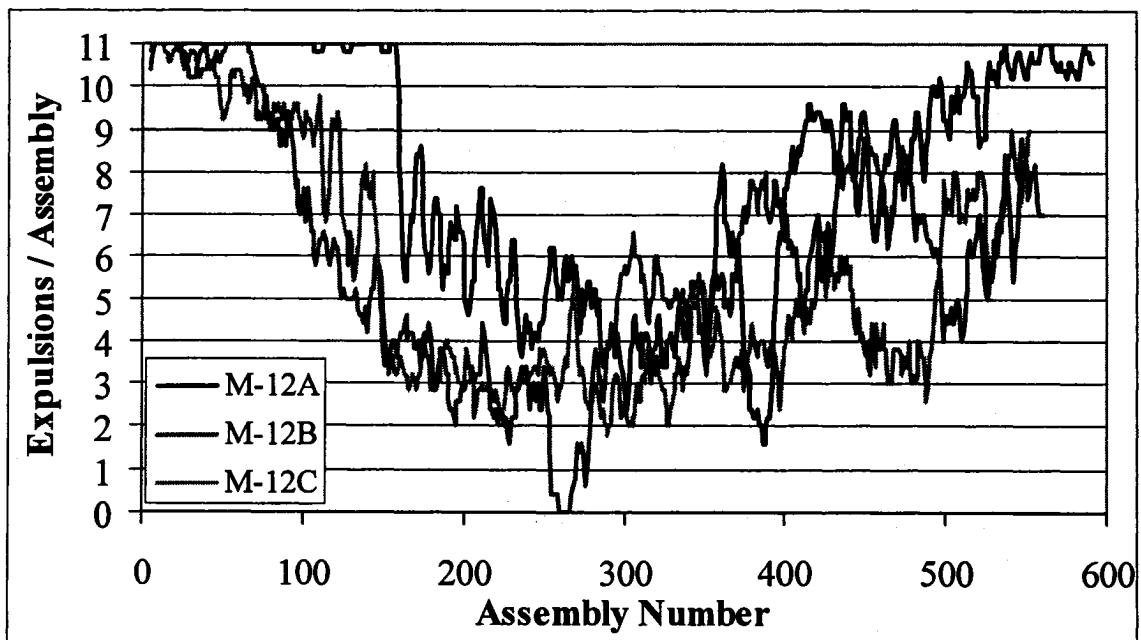


Figure 19: Expulsion observations for the M-12hr trials

4.2.3 Expulsion Observations - FIN Electrode

The starting current for the FIN electrode was selected as 8300 A based on the current range results. The first step in the development of a weld schedule was expulsion observations using the 0.65, 0.75, 0.85 stepper schedule developed for the M electrode. Figure 20 shows that significant expulsion was experienced with these settings. Lowering the stepper rate to 0.5 A per weld resulted in no appreciable decline in the expulsion frequency.

The stepper rate was further reduced to an average of 0.4 A per weld. Similar to the M stepper schedule, the first 2500 welds were set at 0.35 A per weld to reduce thermal degradation initially, and the last 2500 welds set at 0.45 A per weld to maintain current density. Figure 21 displays the four 12-hour trials that were conducted with these settings. In all four trials, the expulsion data exhibits moderate scatter about the running average for the first 200 assemblies. Scatter about the average is high beyond 200 assemblies, but expulsion remained largely at a moderate level with no periods of a zero running average.

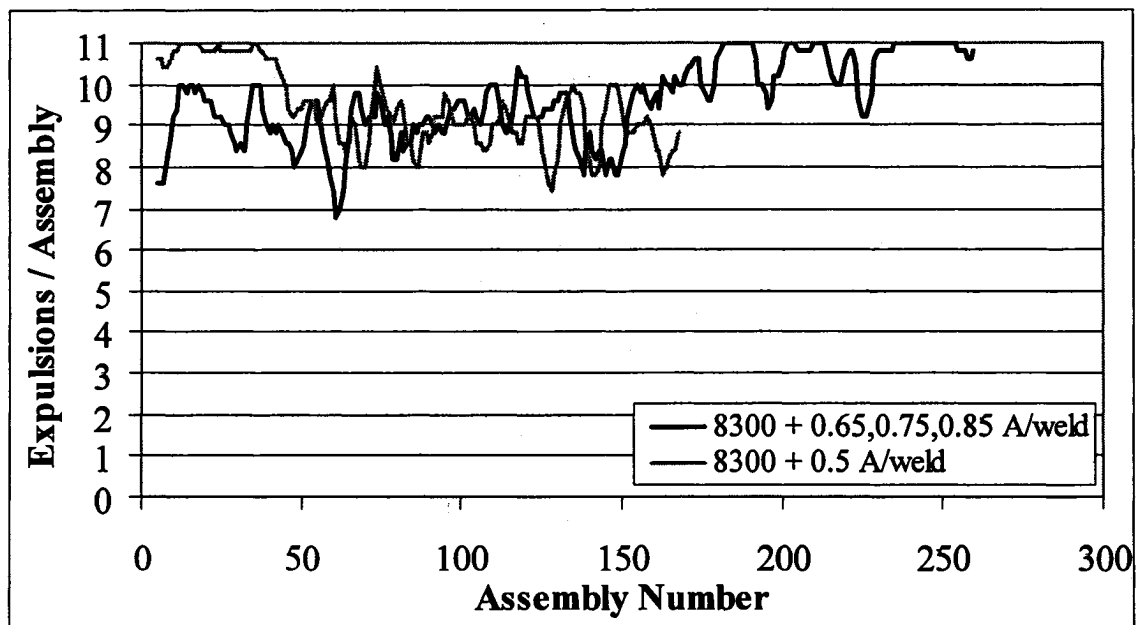


Figure 20: Expulsion observations for the preliminary FIN electrode trials

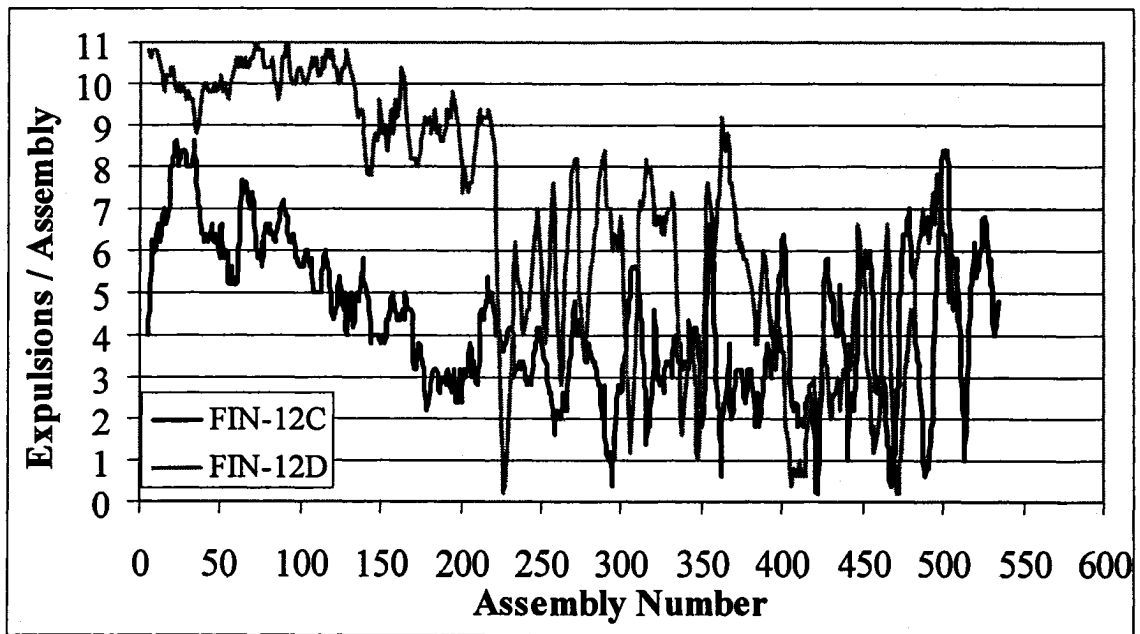
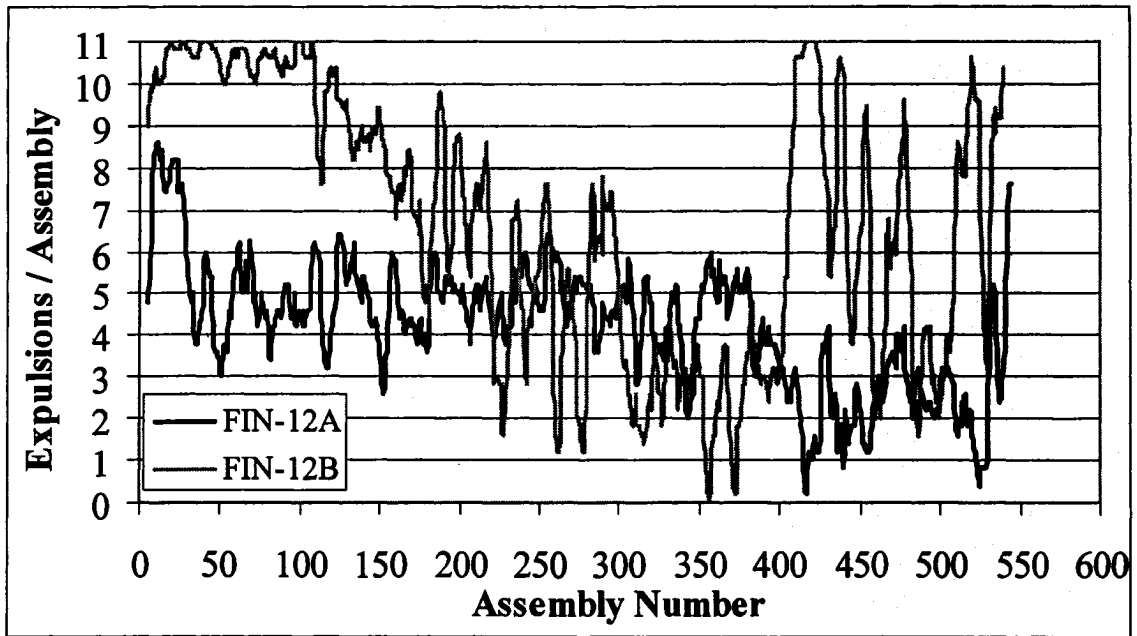


Figure 21: Expulsion observations for the FIN-12hr trials

A 24-hour trial was conducted with the 0.35, 0.40, 0.45 stepper schedule adjusted to account for the extra number of welds. The first 5000 welds were set at 0.35 A per weld, welds 5001-10000 at 0.4 A per weld, and the final 5000 welds set at 0.45 A per weld. Similar to the 12 hour trials, a moderate level of expulsion was maintained for the duration of the trial, as shown in Figure 22, with scatter about the average expulsion value.

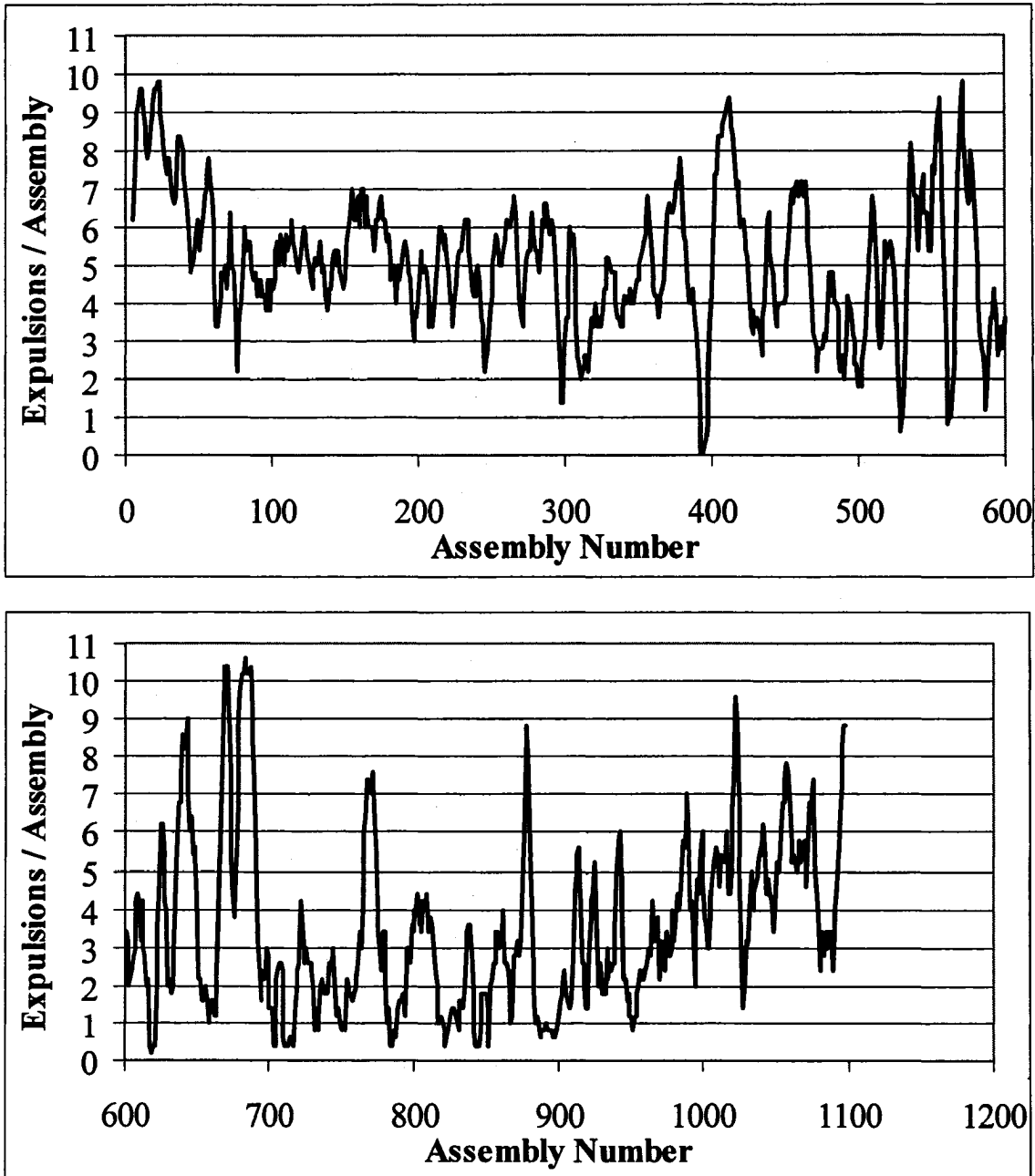


Figure 22: Expulsion observations for the FIN-24hr trial

4.2.4 Expulsion Observations - WAP Electrode

The first step in developing a stepper schedule for the baseline WAP electrode was observing the expulsion behaviour for the existing weld schedule. The expulsion observations were documented on two separate occasions, as shown in Figure 23. It is noted that the two observations produced significantly variable results. During one production run, the running average gradually decreases for the first 150 assemblies and then remains below two. During another production run, nearly full expulsion was experienced for the first 150 assemblies followed by a decrease to a more moderate level.

For the WAP electrode trials, the starting current was programmed to 8250 A following the current range results. Based on the M electrode results, the first trial for the WAP electrode was conducted with the 0.65, 0.75, 0.85 stepper schedule. The expulsion graph, as shown in Figure 24, illustrates that the running average gradually decreases initially followed by several peaks and bottoms. Throughout the duration of the trial, blue *flashes* were consistently noted after the completion of hold time. It was believed that the flashes may have been caused by an insufficient hold time. As well, the electrode exhibited signs of extreme pitting and wear upon removal at the end of the trial. Subsequently, the hold time was increased to 4 cycles for the following trials. This change was not expected to have an effect on the number of interfacial expulsions. The blue flashes were not apparent during any of the remaining trials.

For the following trial, the starting current was lowered to 8000 A. The expulsion frequency showed an initial monotonic decrease, followed by periods of several assemblies without any instances of expulsion. The slight increase in expulsions near the end of the trial was a result of two manual current increases of 250 A each. The weld quality checks during this period were satisfactory.

Subsequent to the results of the previous trial, the starting current was increased to a more conservative 8500 A. Inconsistent performance was noted for the three trials conducted with this starting current, as shown in Figure 25. The WAP3 trial experienced the earliest expulsion drop-off and the running average largely remained below two expulsions for the rest of the trial. The WAP4 did not experience an abrupt expulsion decrease until 175 assemblies and then remained at moderate levels. The WAP5 displayed an expulsion drop-off around 100 assemblies followed by periods of several

assemblies without expulsion. Another inconsistency between the trials was the behaviour of the expulsions themselves. The expulsions for the WAP4 trial were noted to be very light in comparison to the other two trials.

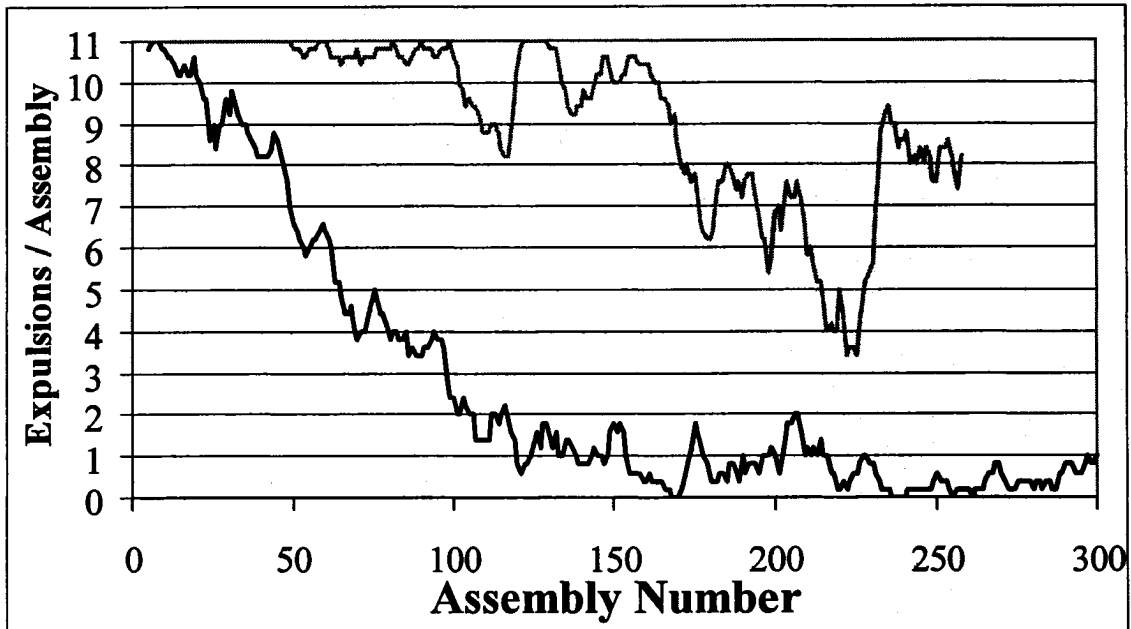


Figure 23: Baseline expulsion observations for the WAP electrode

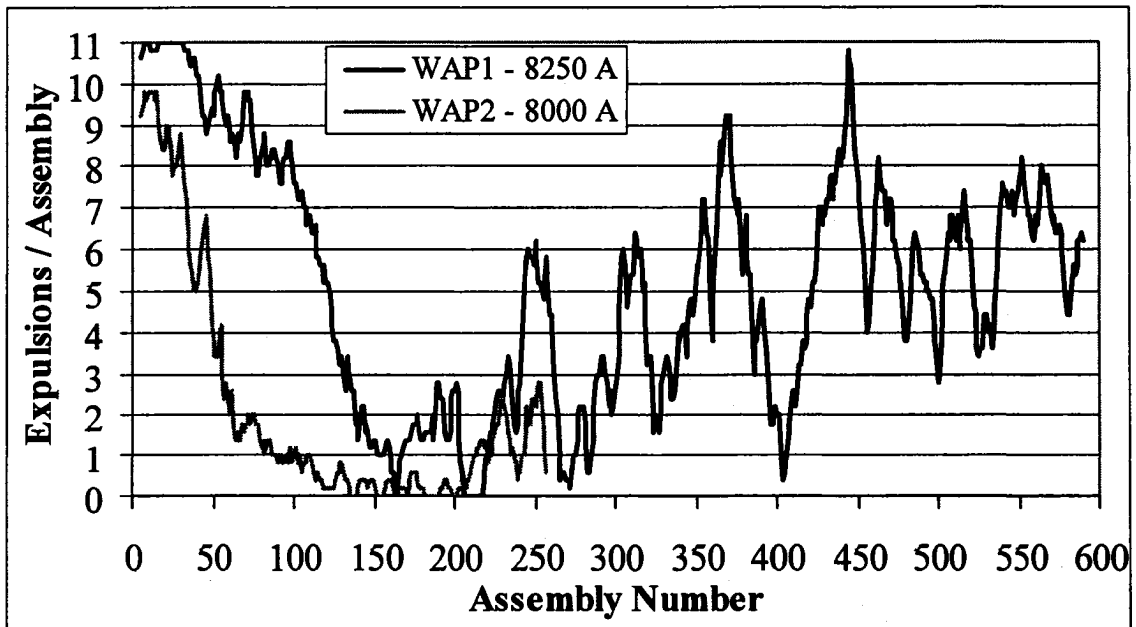


Figure 24: Expulsion observations for the preliminary WAP electrode trials

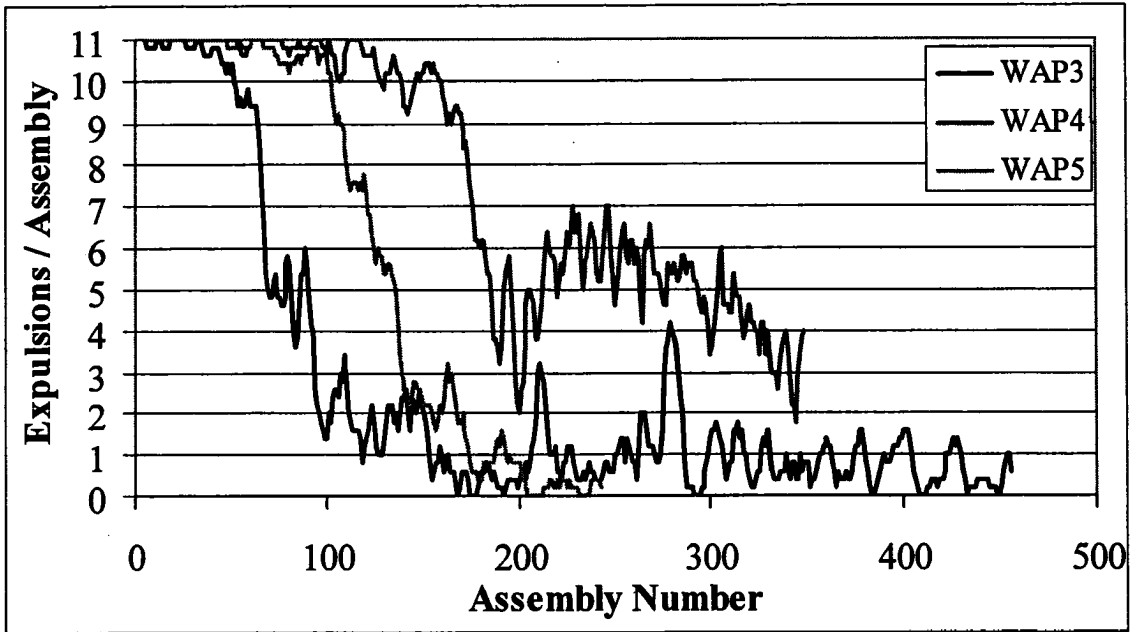


Figure 25: Expulsion observations for the WAP electrode trials conducted with an 8500 A start current and 0.65, 0.75, 0.85 A per weld stepper schedule

4.3 Electrode Face Images

Following both the laboratory and production testing, the electrodes were examined at low magnification to observe the topography of the electrode face. The final condition of the electrode face was recorded through digital imaging. Each of the electrodes showed a significant increase in face contact area at the completion of testing. The final electrode face diameter was determined from the digital images using a circle of best-fit method.

The electrode face images for the GM stepper tests are presented in Figure 26. All of the electrodes exhibited centralized pitting and alloy layer build-up at the periphery of the electrode face. The coarse topography of the electrode faces is evident in each of the images. The electrodes are also characterized by an annular groove at the outer diameter of the electrode face. The final electrode face diameters for the GM stepper tests are provided in Table 8. The measurements reveal that the FIN had the largest face diameters of the three electrode sets. The M electrode displayed the least variation in diameter between the top and bottom electrodes.

The final electrode face diameters for the DCX beta-site trials electrodes are presented in Table 9. The diameters of the top electrodes were larger than the bottom electrodes in every case. The electrode face images for the DCX beta-site trials are presented in Figures 27 to 29. The M-12 electrodes were characterized by centralized pitting, a concave electrode face, and a coarse topography. Evident in the images is the non-circular nature of the outer diameter in certain segments around the face. The FIN-12 electrodes were much more flat and smooth compared to the other electrodes. Smaller delocalized pits can be seen across the electrode face as well as mushroomed wings at the periphery. The FIN-24 electrodes displayed a rougher topography and more significant pitting compared to the FIN-12 electrodes. The WAP1 electrodes exhibited the most severe form of centralized pitting. The face of the WAP1 top electrode was covered with copper-containing debris at two locations along the periphery extending in a radial direction toward the centre of the face.

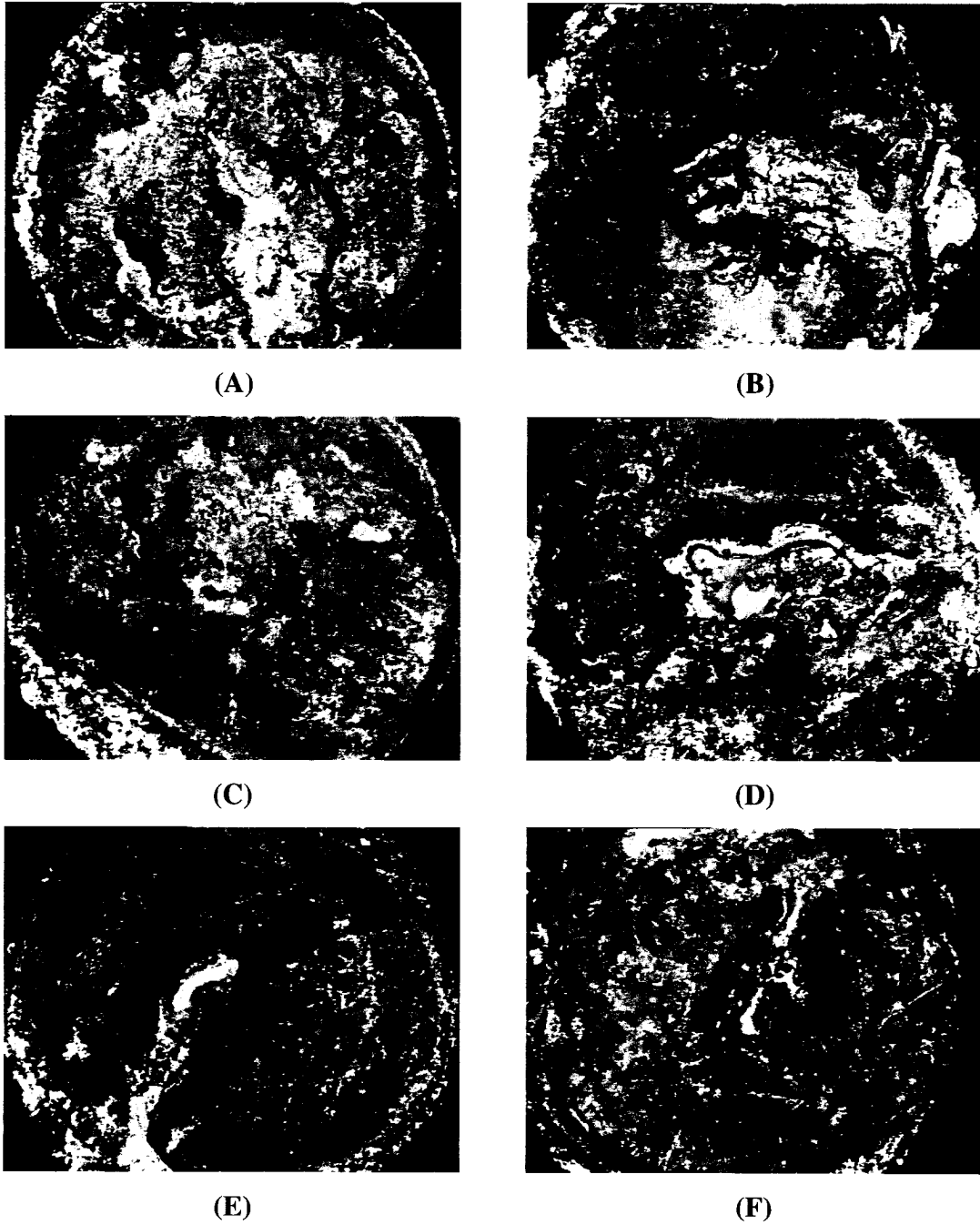


Figure 26: GM stepper tests end-of-life electrode face images: CuZr (A) Top (B) Bottom; M (C) Top (D) Bottom; and FIN (E) Top (F) Bottom

Electrode	# welds	Top Diameter	Bottom Diameter
CuZr	8500	9.319	9.816
M	7500	9.675	9.591
FIN	7000	9.821	10.173

Table 8: Summary of electrode face diameters (mm) for the GM stepper tests

Electrode	# welds	Top Diameter	Bottom Diameter
M-12A	6501	7.769	7.574
M-12B	6171	7.490	7.267
M-12C	6072	7.493	7.271
FIN-12A	5984	7.445	6.942
FIN-12B	5929	7.546	7.071
FIN-12C	5874	7.295	6.848
FIN-12D	5599	7.350	6.681
FIN-24	12078	9.033	8.677
WAP1	6490	8.255	7.640
WAP3	5016	7.494	6.936

Table 9: Summary of electrode face diameters (mm) for the DCX beta-site trials

The electrodes from the GM stepper tests exhibited more significant pitting and wear compared to the DCX beta-site electrodes. This can be attributed to the more severe condition of welding hot-dipped galvanized steel compared to galvanized steel. The rate of electrode face enlargement is addressed in the discussion.

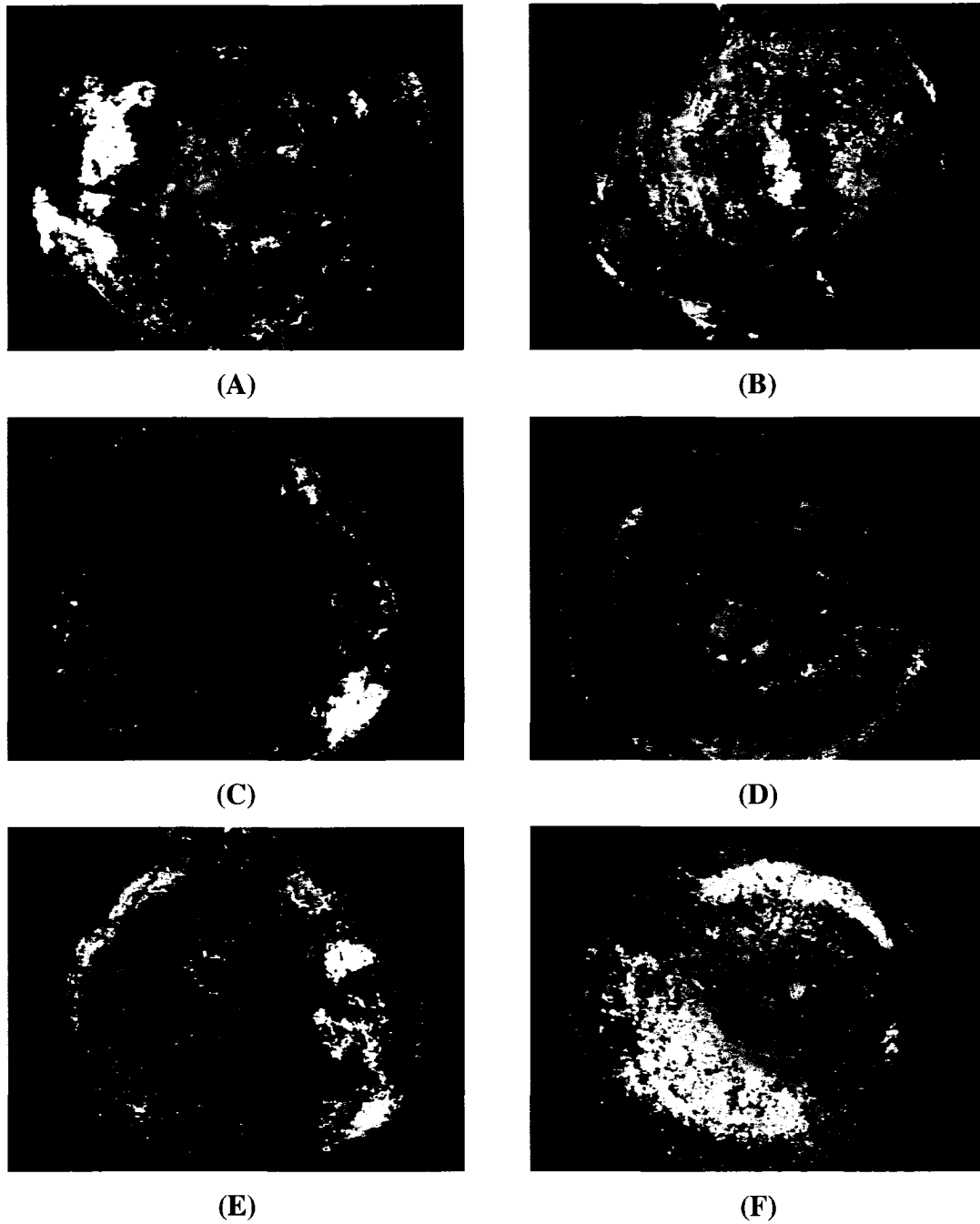


Figure 27: Electrode face images for the M electrode trials: M-12A (A) Top (B) Bottom; M-12B (C) Top (D) Bottom; M-12C (E) Top (F) Bottom

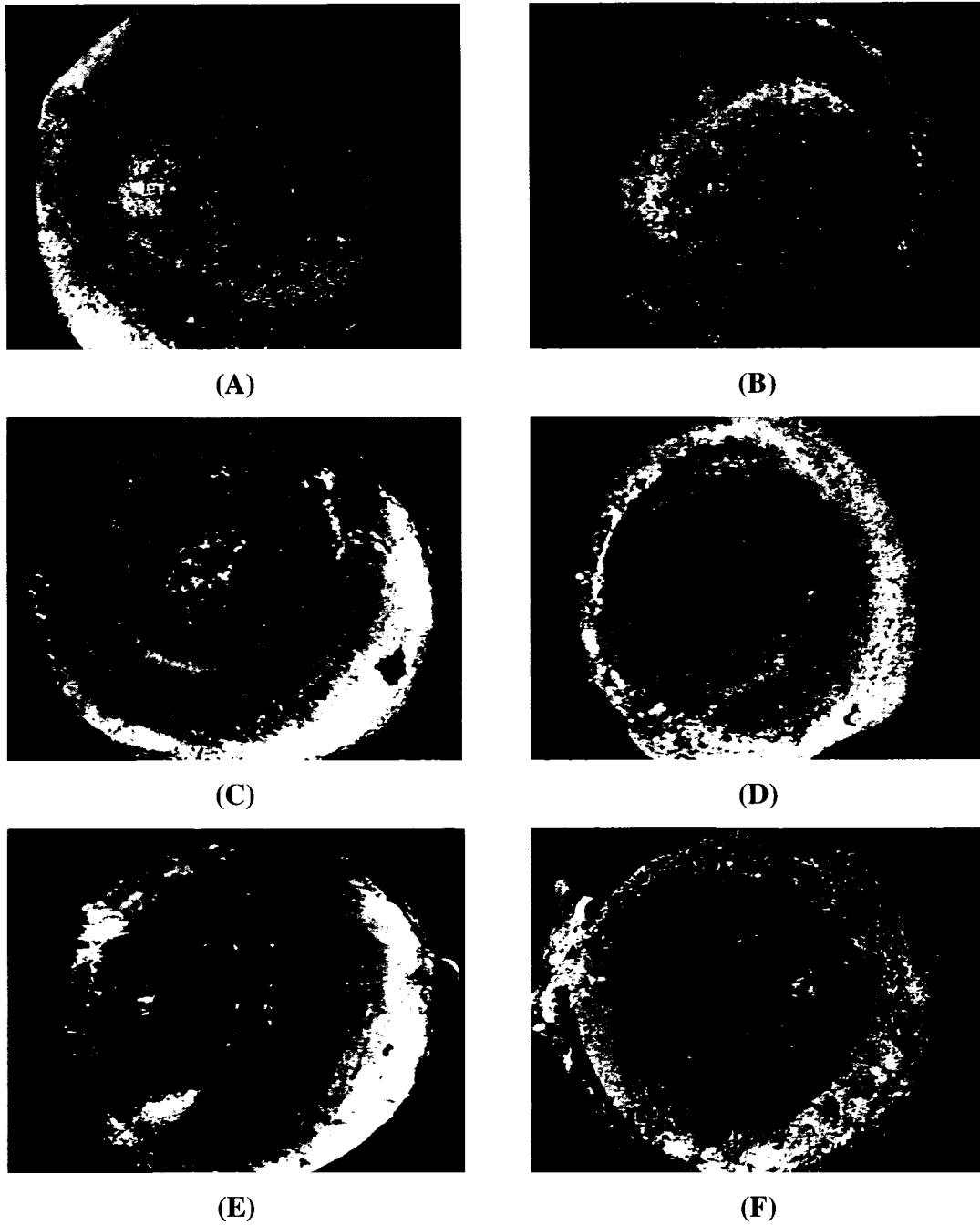
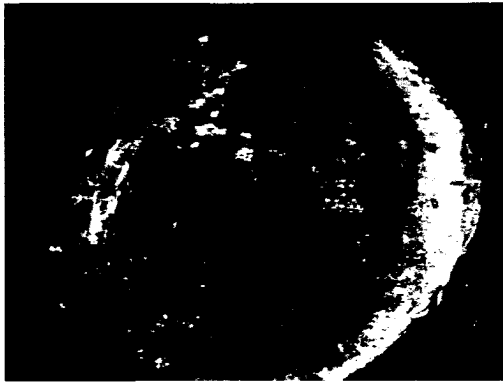
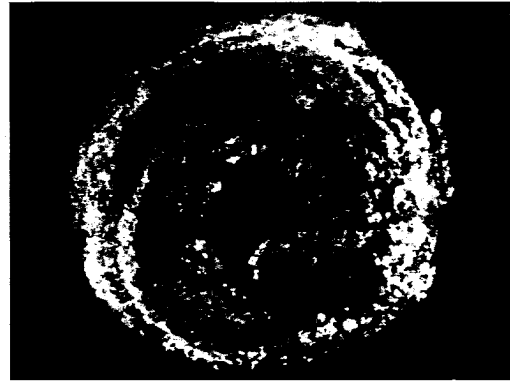


Figure 28: Electrode face images for the FIN electrode trials: FIN-12A (A) Top (B) Bottom; FIN-12B (C) Top (D) Bottom; FIN-12C (E) Top (F) Bottom;



(G)



(H)

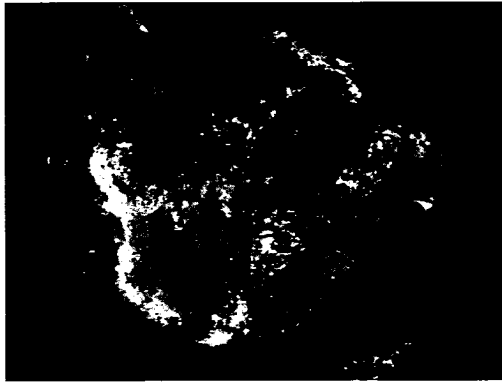


(I)

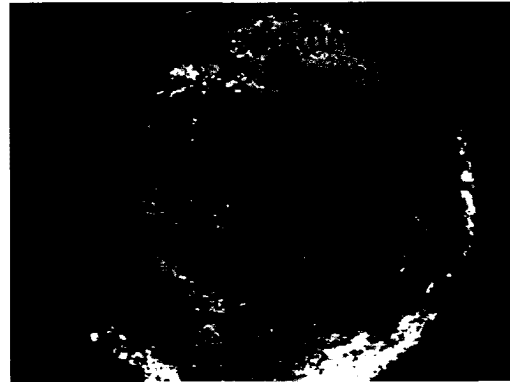


(J)

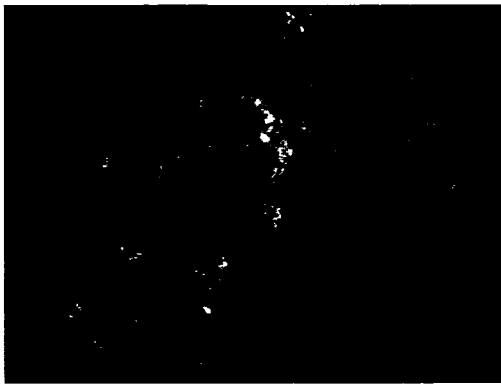
Figure 28 continued: FIN-12D (G) Top (H) Bottom; FIN-24 (I) Top (J) Bottom



(A)



(B)



(C)



(D)

Figure 29: Electrode face images for the WAP electrode trials: WAP1 (A) Top (B) Bottom; WAP3 (C) Top (D) Bottom

4.4 Metallographic Evaluation

Following laboratory and production testing, the electrodes were examined using standard metallographic techniques. Vickers microhardness testing was conducted to determine the depth of softening beneath the electrode face. The average thickness of the individual brass-alloy layers was determined via optical microscopy. Etching was completed to reveal the microstructure and any evidence of recrystallization near the electrode face.

4.4.1 Microhardness Results

Electrodes lose their hardness at the face as a result of prolonged thermal degradation. Softening in precipitation hardened electrode materials can be attributed to dissolution or overaging of precipitates and or recrystallization. Less softening is experienced by oxide dispersion strengthened materials because the dispersoids used to strengthen the base copper are stable at elevated temperatures. However, the welding heat does provide enough energy to allow dislocation climb to defeat the dispersion strengthening mechanism and cause some softening [7].

Room temperature hardness traces for the GM stepper electrodes are shown in Figures 30 and 31. The hardness drop for each of the electrodes is greater at the centre than at the edge of the face. The most significant hardness drop was exhibited by the CuZr and FIN electrodes. At the centre, the depth of softening for both electrodes extends 2 mm into the electrode body with the hardness of the FIN on average 12 HV below that of the CuZr. At the edge, the CuZr has maintained its hardness up to 0.5 mm from the electrode face while the FIN shows the same 2 mm softening depth. The M experienced only a slight hardness drop at either the centre or the edge.

Hardness values from the DCX beta-site trials are displayed in Figures 32 and 33. Again, the hardness drop at the centre of the face is greater than at the edge. At the centre, the FIN-24 is about 10 HV softer than the FIN-12 up to a depth of 1 mm. At the edge, the FIN-24 exhibited more significant softening than the FIN-12 up to a depth of 0.3 mm. Similar to the GM stepper test, the M-12 experienced only a slight hardness drop at either the centre or edge. The WAP1 electrode was best able to maintain its hardness and did not experience any softening at either the centre or edge.

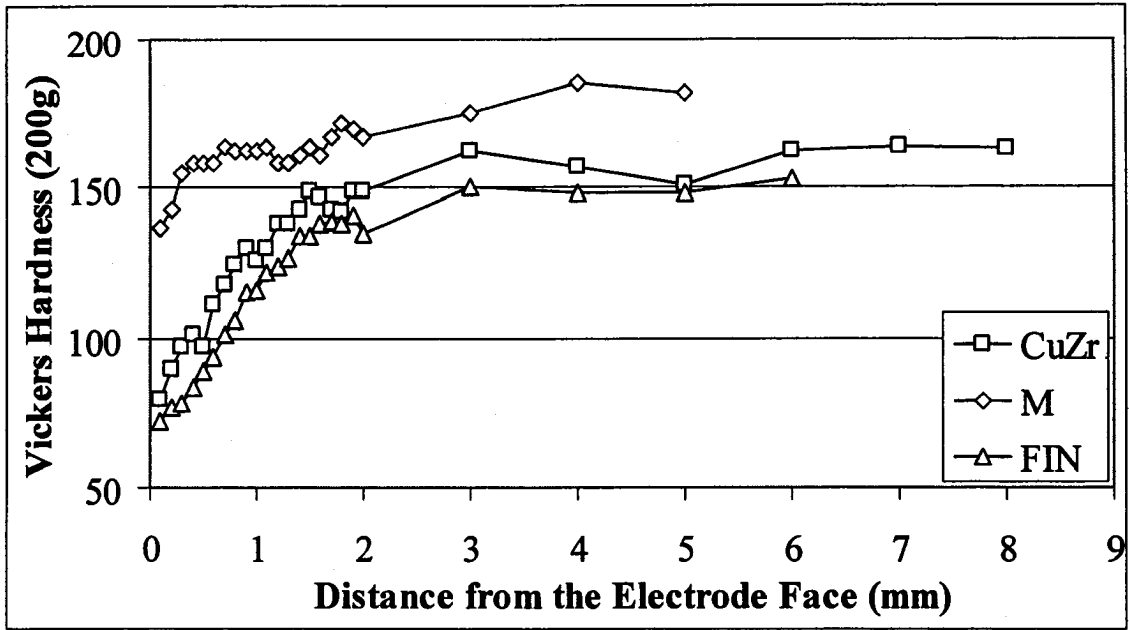


Figure 30: Hardness values at the face centre for the GM stepper tests electrodes

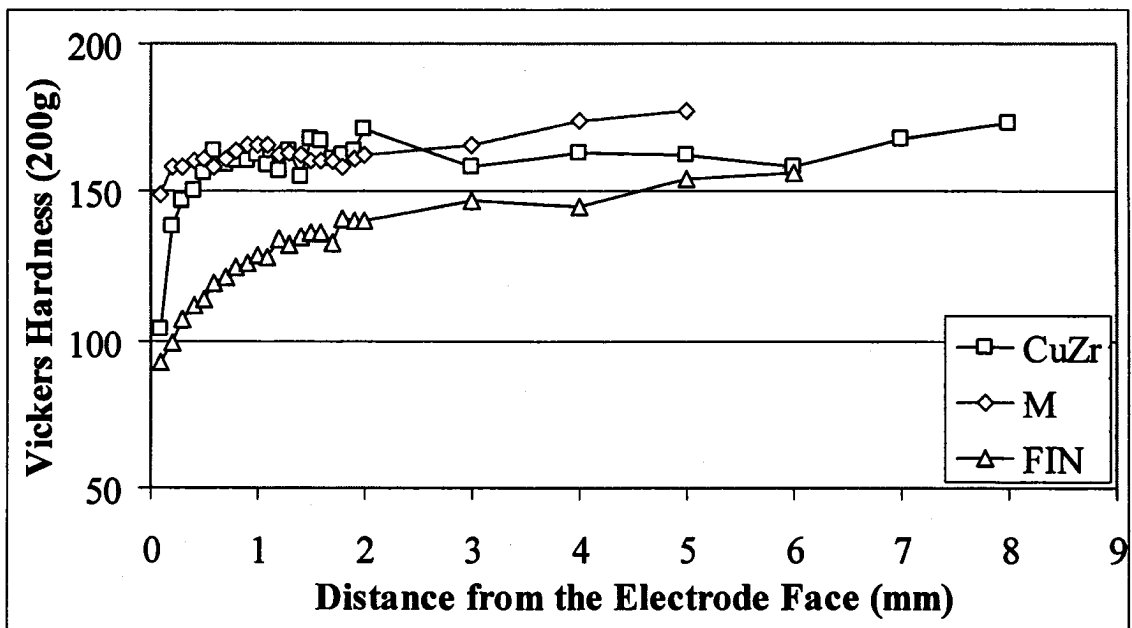


Figure 31: Hardness values at the face edge for the GM stepper tests electrodes

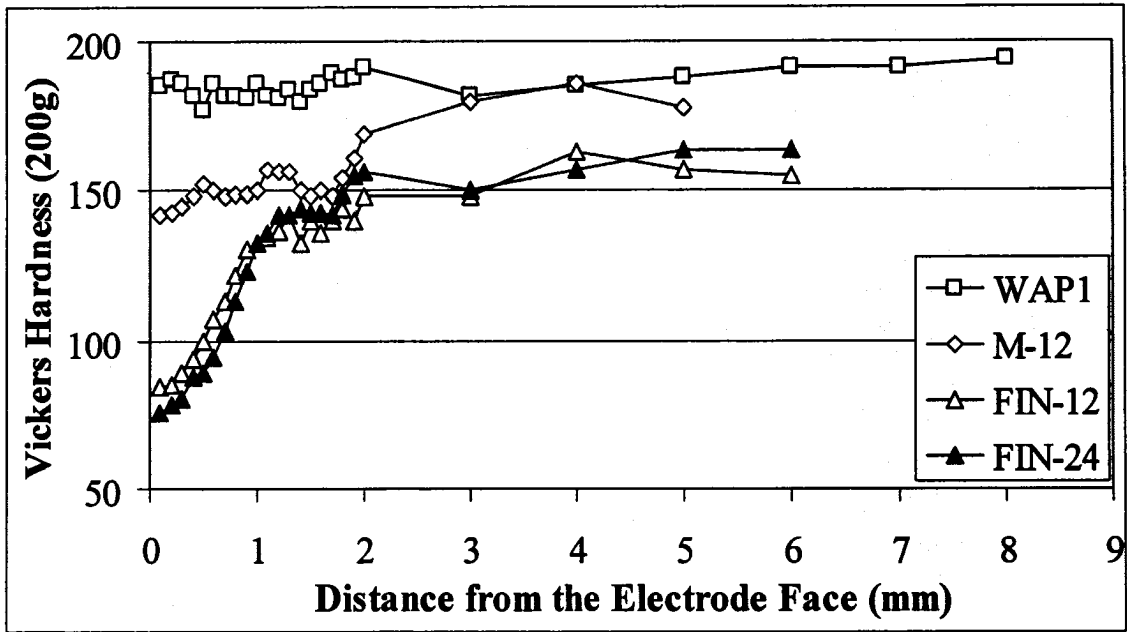


Figure 32: Hardness values at the face centre for the DCX beta-site trials electrodes

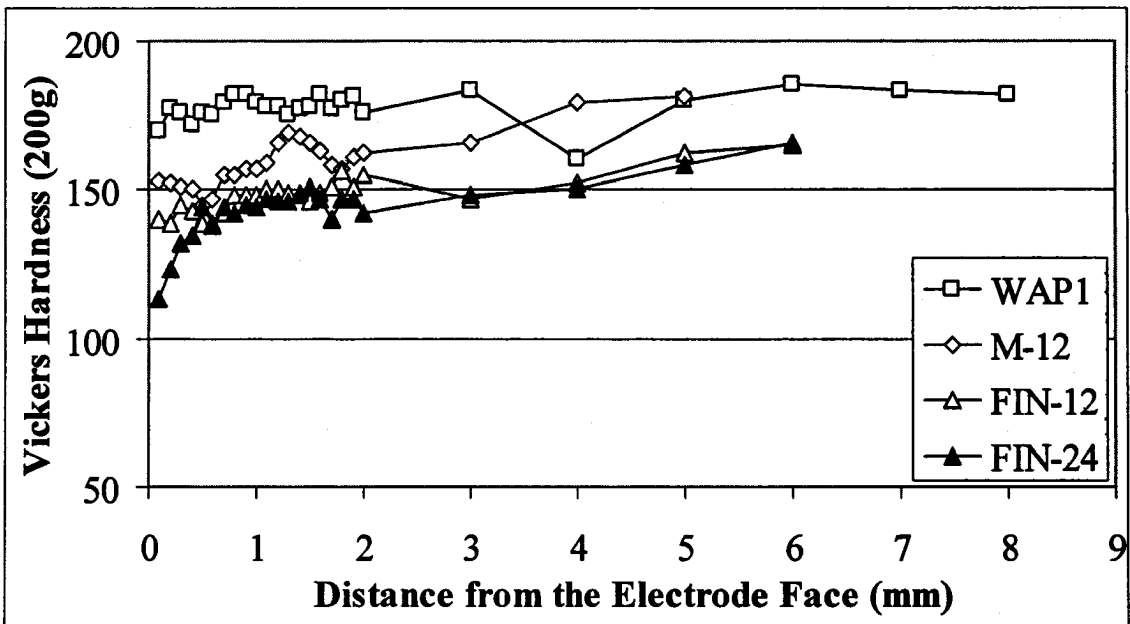


Figure 33: Hardness values at the face edge for the DCX beta-site trials electrodes

4.4.2 Alloy Layer Thickness Measurements

Alloy layer thickness measurements for the GM stepper tests electrodes are presented in Figure 34. There was little variation among the electrodes in the thickness of the individual alloy layers. The total thickness of the two brass layers was found to be approximately 15 μm for each electrode. The thickness of the parting layer was more variable than the brass-alloy layers. The M electrode displayed the thickest parting layer of the three electrodes. The optically distinct beta-brass, gamma-brass, and parting layers are shown in Figure 35.

The alloy layer thicknesses for the DCX beta-site trials electrodes are also presented in Figure 34. Individual measurements across the entire face diameter revealed that the FIN-12 and FIN-24 electrodes exhibited a more consistent point-to-point alloy layer thickness than the M-12 or WAP1 electrodes. Comparable to the GM stepper tests, the total thickness of the beta- and gamma- brass layers was nearly equivalent for the M-12 and FIN-12. The FIN-12 exhibited a slightly smaller beta layer and a slightly larger gamma layer compared to the M-12. The thickness of the individual brass alloy layers was found to be slightly greater for the FIN-24 compared to the FIN-12. The WAP1 displayed the thickest alloy layers, particularly the parting layer, of all the electrodes. With an average thickness of 30 μm , the parting layer represents over half of the total alloy layer thickness for this electrode.

Figure 36 reveals a mixed layer present at the interface of the parting and gamma-brass layers in a FIN-12 electrode. This mixed layer was predominant at the central portion of the electrode face and was not evident near the edges. The average thickness of the mixed layer was found to be 40 μm , much greater than the other alloy layers. This observation raises the possibility that the mixed layer represents a protrusion, which is an extension of the central portion of the electrode face. Lu et al. [16] also observed the formation of a protrusion when welding galvanized steel with a copper-zirconium electrode. The mixing of beta- and gamma-brass layers has been previously noted by Athwal [17].

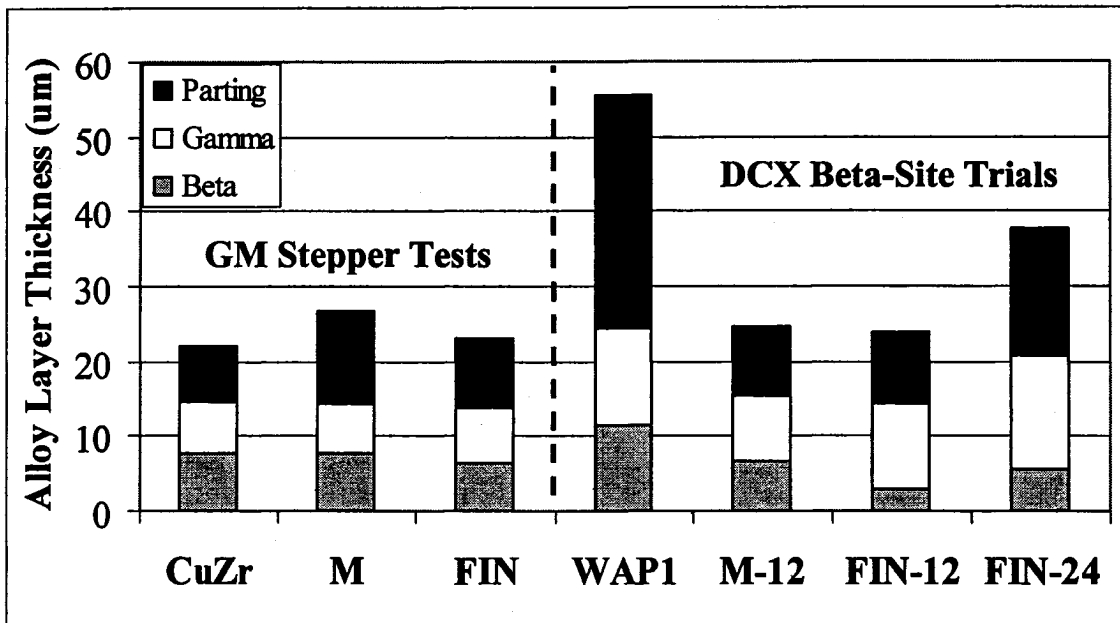


Figure 34: Alloy layer thickness measurements for both the GM stepper tests electrodes and the DCX beta-site trials electrodes

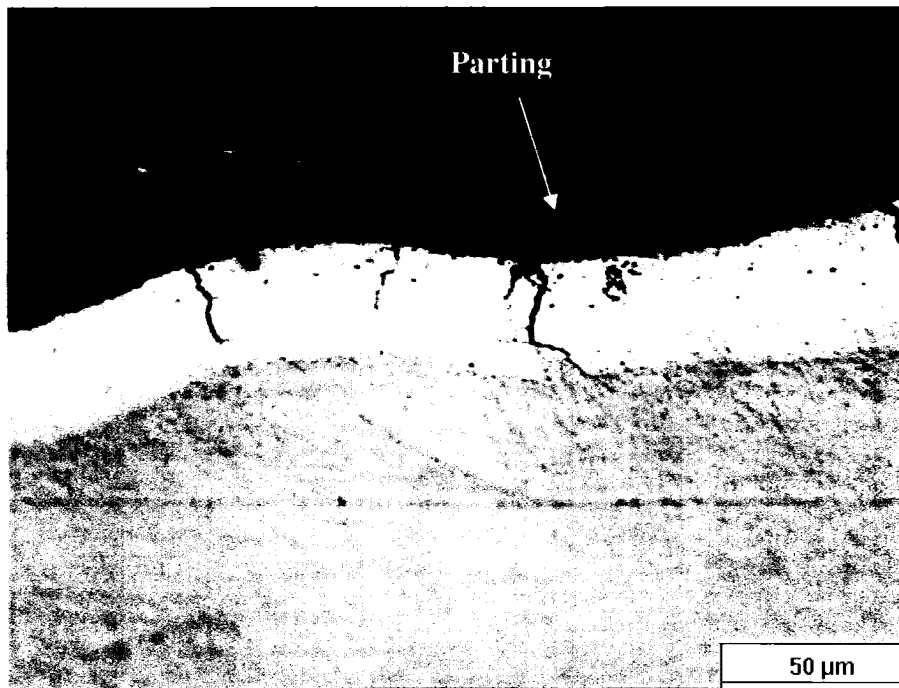


Figure 35: Optically distinct beta-brass (yellow), gamma-brass (white), and parting layers in the FIN-24 electrode



Figure 36: Mixing of the parting and gamma-brass layers in a FIN-12 electrode. The mixed layer had an average thickness of 40 μm and was only evident at the centre of the electrode face.

4.4.3 Microstructural Observations

Recrystallization was apparent near the electrode face for the precipitation hardened electrode materials, namely the CuZr and FIN electrodes. Recrystallization was most prevalent near the centre of the electrode face, but was also observed near the edges. This observation is consistent with the lower hardness values noted at the centre of the electrode face. The depth of recrystallization varied across the electrode face; the average depth of recrystallization was 150 μm . The deepest and most extensive recrystallization was found in the FIN-24 electrode. Figure 37 shows the forged microstructure of the electrode body giving way to smaller equiaxed grains near the electrode face. Significant grain growth does not appear to have occurred due to the dispersion of the copper-zirconium precipitates. As expected, the M electrode resisted recrystallization at the electrode face, as shown in Figure 38.

Figure 39 shows a double crack intersecting a central pit in an M-12 electrode. The current concentration around the crack may have aided in the formation of the pit. The larger of the two cracks extends 1.5mm into the electrode body. Alloying was also noted to occur along the crack near the electrode face. Cracking has been previously noted for this material without an apparent effect on electrode life [17].

The formation of a wing at the edge of the electrode face is shown in Figure 40 for a FIN-12 electrode. Wing formation at the edge of the electrode face was far more extensive for the FIN-12 electrodes than the M-12 electrodes. Optical metallography revealed that both the underlying copper material and the brass-alloys layers were extruded to form the wing.

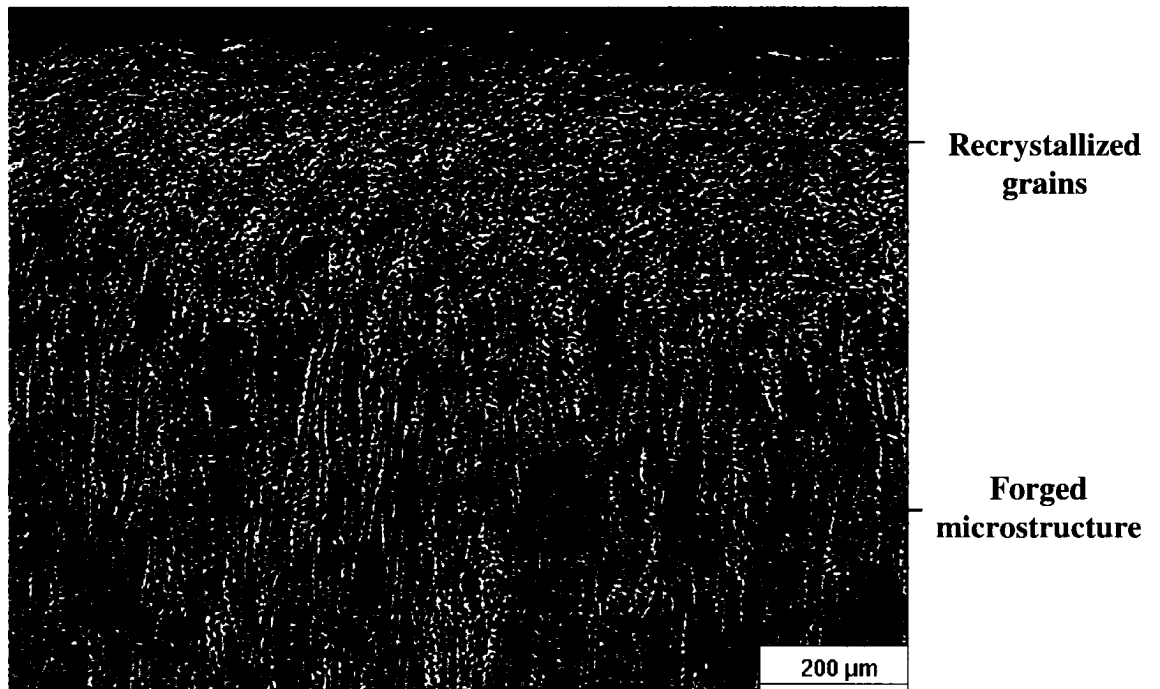


Figure 37: Recrystallization at the centre of the electrode face for the FIN-24 electrode. The figure shows the forged microstructure of the electrode body giving way to recrystallized grains near the face.

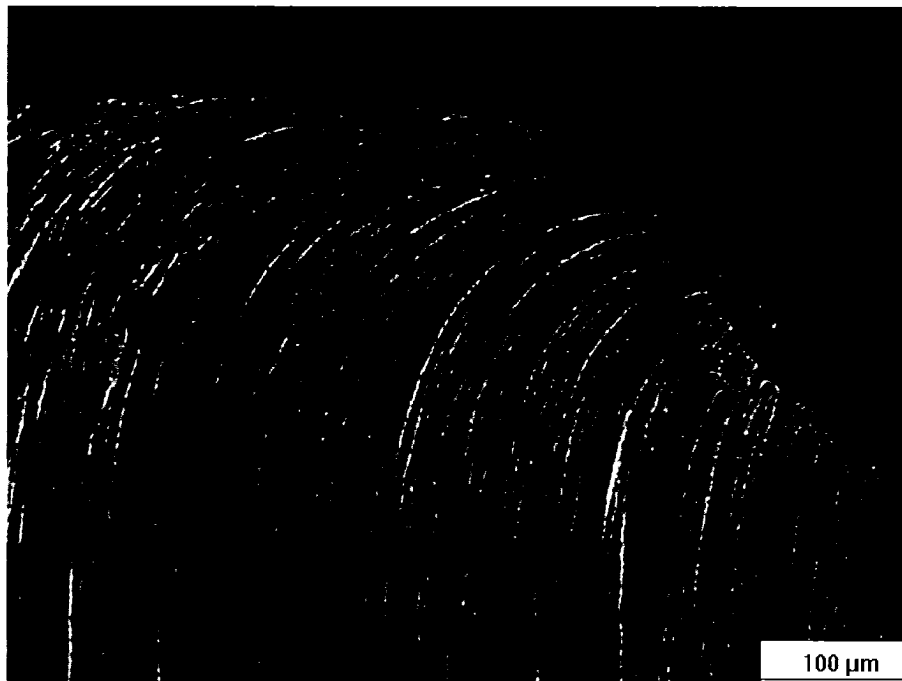


Figure 38: Deformation pattern of an M-12 electrode which shows no evidence of recrystallization at the edge of the electrode face

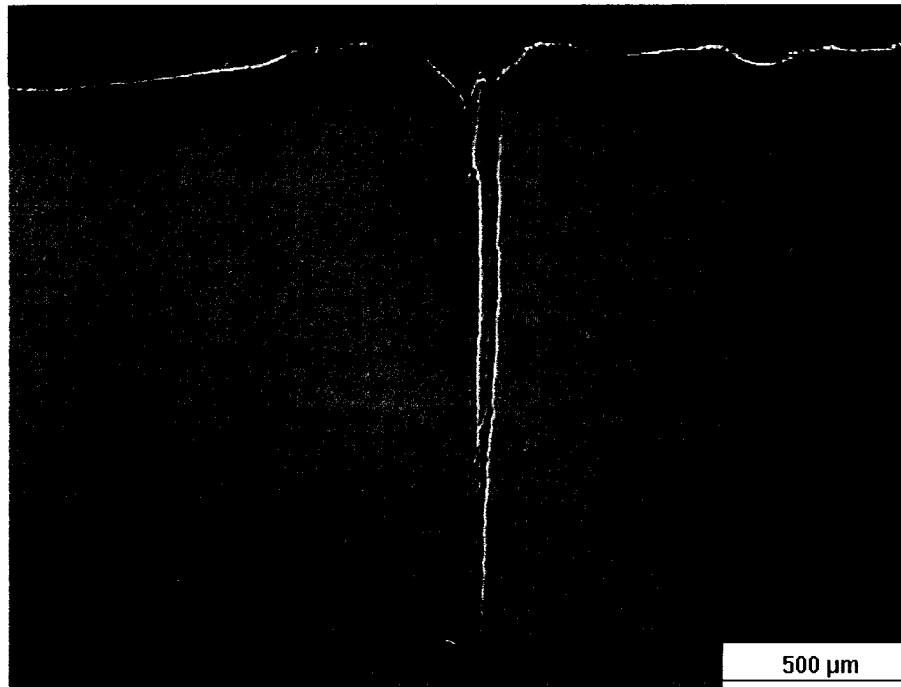


Figure 39: A double crack intersecting a central pit in an M-12 electrode. The larger of the two cracks extends 1.5 mm into the electrode body.

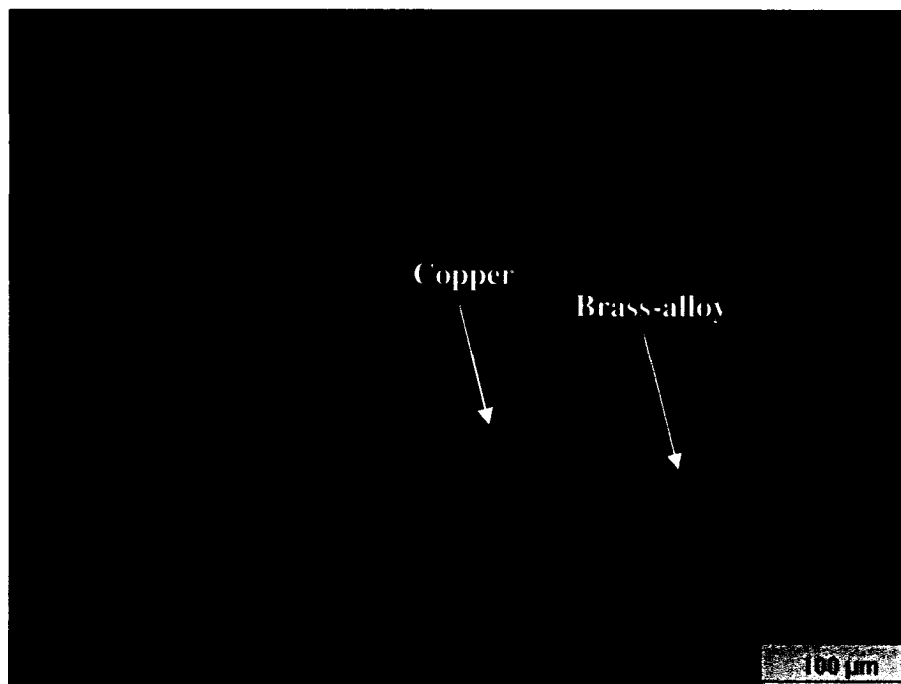


Figure 40: Extensive wing formation in a FIN-12 electrode showing both brass-alloy extrusion and copper extrusion at the edge of the electrode face

V. DISCUSSION

This section first discusses the overall results from the laboratory and production tests. The rate of electrode face enlargement is then discussed along with the associated current density requirements for maintaining weld quality. A detailed analysis of electrode cooling is given to highlight its importance in limiting thermal degradation and electrode face enlargement. Finally, a methodology for developing production weld schedules along with its associated benefits is presented.

5.1 Comparison of Test Results

The results from the GM stepper tests reveal the baseline CuZr to have the longest electrode life of 8500 welds, followed by the M and FIN at 7500 and 7000 welds respectively. The CuZr also required the lowest stepper rate and produced the least number of no-weld dropouts of the three electrodes. Overall, for the given laboratory test conditions, the developmental electrodes were outperformed by the CuZr, a widely used electrode in the automotive industry.

The results from the DCX beta-site trials showed that both the M and the FIN were able to show repeatable performance in a production environment. The electrodes consistently maintained moderate levels of expulsion during consecutive trials with the same weld schedule. In terms of lower current levels, both of the developmental electrodes were able to outperform the baseline WAP electrode. The FIN was the best performing electrode, as it required a significantly lower stepper rate than its competitors.

Both testing evaluations involved increasing the weld current as the electrode face enlarged from repeated welding. A mean stepper rate of 0.75 A per weld was achieved for the M electrode in both the laboratory and production testing. For the FIN electrode, a substantially lower stepper rate of 0.4 A per weld was required in the production trials compared to the 0.99 A per weld for the laboratory tests. However, there were several key differences between the two tests including the type of steel welded, cooling-water flow rate, weld time, electrode force, and number of welds. Each of these factors would play a significant role in electrode wear and subsequently electrode performance.

5.2 Electrode Face Enlargement

Electrode face enlargement when welding galvanized steels occurs from a combination of chemical and mechanical erosion. Mechanical erosion occurs from the extrusion of both brass alloys and base copper to the periphery of the electrode face. Chemical erosion occurs from the loss of copper material as it is transferred onto the sheet surface in the form of brassing. The electrode face diameter increases from chemical erosion as a consequence of electrode geometry. When mechanical erosion and/or chemical erosion are limited, the rate of electrode face enlargement is reduced.

The rate of electrode face diameter increase is provided in Table 10 for the two testing conditions. The production values represent an average taken from the 12-hour trials. The rate of electrode face diameter increase was much greater for the GM stepper tests. This can be attributed to higher levels of mechanical and chemical erosion given the welding conditions of the laboratory tests. Holliday et al. [38] have shown that the loss of copper material from the electrode face, and thus chemical erosion, is greater for hot-dipped galvanized than for galvanized steel. Greater mechanical erosion would occur given the higher electrode force of 670 lbf compared to 380 lbf for the production trials. Furthermore, a longer weld time and lower cooling-water flow rate would have exposed the electrodes to higher levels of thermal degradation. The total combination of these conditions would clearly lead to a higher rate of electrode face diameter increase.

Electrode	Rate of Electrode Face Diameter Increase ($\mu\text{m}/\text{weld}$)	
	GM Stepper Tests	DCX Beta-Site Trials
M	0.644	0.428
FIN	0.742	0.401

Table 10: Rate of electrode face diameter increase for each testing condition

Howes and Lake [35] have noted that electrode life during production welding is governed by the rate of electrode face enlargement with increasing numbers of welds. The improved performance of the FIN in the production trials can be attributed to a much lower rate of electrode face enlargement than for the laboratory tests. Any limitation in

thermal degradation would be expected to have a greater effect on the FIN than the M, because the FIN has a lower strength and thereby a greater propensity for mushrooming.

The formation of wings was far more extensive for the FIN-12 electrodes in spite of their lower rate of electrode face enlargement in the production trials. Given that the formation of wings represents mechanical erosion, this may point to chemical erosion as being the dominant electrode wear mechanism, as previously noted by Gallagher [7]. This may also reveal that improved electrode cooling more significantly limits chemical erosion than mechanical erosion.

5.3 Current Density Requirements

While resistive heat generation is directly related to the square of the weld current, melting at the faying interface will not occur without a concentration of the current. The electrode wear process is marked by elevated levels of thermal degradation leading to a substantially enlarged electrode face. An increased electrode face diameter requires that weld current be increased to maintain the necessary current density.

In the GM stepper tests, weld current was increased when minimum button size was not achieved in the 100-weld interval check. These increases in weld current were a response to the enlarged electrode face. For the DCX beta-site trials, a pre-programmed start current and stepper rate were employed to anticipate electrode face enlargement. In both cases, weld current was increased to accommodate for the larger face diameter and maintain a certain current density.

Peterson [1] has noted that the balance between achieving acceptable rates of electrode wear while maintaining insensitivity to current density fluctuations is best met at or just below the expulsion current. If current levels are set excessively below expulsion, even small increases in electrode face diameter reduce current density enough to lead to weld size dropouts. Higher than necessary currents, with severe expulsion, subject the electrodes to increased thermal degradation and accelerated electrode wear rates. For the production testing, welding with moderate expulsion was utilized to protect against weld size dropouts. These current levels could sustain suitable weld nugget sizes, even if the electrode face were subject to rapid enlargement.

Table 11 displays the average current density of the top and bottom electrodes at the end-of-life for each of the testing conditions. The values from the production testing represent an average taken from the 12-hour trials. The current density was calculated from the final testing current and the final face diameter. As expected, the current density required to maintain expulsion in the production trials was on average 86 A/mm² higher than that required to maintain minimum button size during the laboratory testing. The values also show that the current density of the M was on average 31 A/mm² greater than the FIN. The lower required current density for the FIN may be a consequence of its higher electrical conductivity.

The minimum current density to produce acceptable minimum sized welds was noted by Gallagher [7] to be at least 200 A/mm². As well, Peterson [2] found that electrodes tend toward a 225 A/mm² current density limit as electrode wear progresses. The current density for the M agrees quite well with the above values; the current density of the FIN is lower than expected. This lower value may be a result of the different techniques used to determine the electrode face diameter. For the above current density values, carbon imprints of the electrode face were used to determine the face diameter. In this study, digital images of the electrode face were used to determine the face diameter. It was noted that when compared to the carbon imprints, the face diameters from the digital images were slightly greater. This discrepancy would result in a lower calculated current density.

Electrode	Current Density (A/mm ²)	
	GM Stepper Tests	DCX Beta-Site Trials
M	210	298
FIN	181	265

Table 11: End-of-life current density comparison

5.4 The Importance of Electrode Cooling

Electrode cooling is achieved via heat diffusion in the copper through conduction and heat extraction by the cooling-water through convection. Heat from the welding operation is conducted through the electrode and is coupled with the cooling-water at the

water channel interface. Thermal degradation of the electrode is related to the maximum temperature experienced by the electrode as well as the time spent at maximum temperature. Enhanced cooling limits thermal degradation by restricting chemical erosion from brassing and mechanical erosion from elevated-temperature mushrooming.

Reducing the electrode face thickness positions the water channel closer to the highest temperatures experienced at the electrode face. Maximum cooling occurs when the balance between conduction and convection is optimized through the electrode face thickness. When the face thickness is larger than necessary, less cooling is achieved by the cooling-water since the heat must diffuse a longer distance before it reaches the water channel [46]. If the face thickness is too thin, heat builds up near the electrode face as a result of the reduced thermal mass of the copper electrode.

A low cooling-water flow rate, such as the 0.5 gpm used in the GM stepper tests, combined with a small face thickness can result in electrode overheating. Evidence of boiled cooling-water was apparent for the M electrode at the end of GM stepper test. A white residue, as shown in Figures 41 and 42, was deposited on the inside face of both the top and bottom electrodes. In addition, a reverberating noise characteristic of boiling cooling-water was noted by the welding technician during the test. This residue was not evident for either the CuZr or FIN electrodes, each of which had larger face thicknesses. Furthermore, the white residue was not found on any of the M electrodes tested during the DCX beta-site trials. This observation suggests that the optimum face thickness for electrode cooling is greater than 6 mm for a cooling-water flow rate of 0.5 gpm and that the optimum thickness decreases with higher cooling-water flow rates.

The addition of fins inside the water channel increases the rate of convective heat transfer in two ways. Primarily, the fins increase the water channel surface area that is available for convective heat transfer. For the FIN electrode, the fins increased the surface area by approximately 50 percent, resulting in a proportional increase in the rate of convective heat transfer. Secondly, the fins also promote turbulent flow of the cooling-water, significantly increasing the convection heat transfer coefficient [47].

Another important variable affecting electrode cooling is the flow rate of the cooling-water. Higher cooling-water flow rates promote turbulent flow and significantly enhance convective heat transfer. The results clearly illustrate that the enhanced cooling

properties offered by the FIN electrode were far more beneficial at the higher water flow rates of the production testing. This correlates with the results from a study by Kim and Eagar [46] which indicated that water flow rate had a greater effect on electrode cooling when the face thickness, and thus the balance between conduction and convection, was optimized.

Experimental and analytical analysis would provide further insight to the enhanced cooling offered by internal fins. Experimental testing could be conducted using two identical electrodes, with and without fins, at various water flow rates to help determine the optimal cooling conditions for electrode life. The analytical analysis could include computer modelling to evaluate the performance of the fins on the basis of enhanced heat transfer relative to a no-fin case.



Figure 41: An untested M electrode (l) and one exhibiting white residue from boiled cooling-water (r). The white residue was not evident for the CuZr or FIN electrodes.



Figure 42: An up-close (29.5X) of the white residue found on the inside face of the M electrode

5.5 Candidate Electrode Material

The results for the M electrode reveal the potential for a new material that has shown consistent performance in both the laboratory and production testing. Although the total electrode life in the GM stepper test was less than the baseline CuZr, this new material did not experience its first no-weld condition until 4300 welds. The CuZr and FIN electrodes, each manufactured from an industry standard copper-zirconium alloy, exhibited no-weld dropouts at 2000 and 1800 welds respectively; this occurrence would represent an effective end-of-life condition in a production environment. The button size stability exhibited by this electrode material was also noted by Athwal [17] for both the AWS endurance test and sequential life testing. Button size consistency is important in a production environment, where predictability in scheduling and maintenance translate into increased productivity. The button size consistency also promotes enhanced weld quality through reliability, and cost savings through a decrease in the over-welding of assemblies.

The results from the production testing provide further evidence of the consistency of the M electrode material. This consistency is readily shown by the expulsion behaviour for the replicate trials conducted with the final developed weld schedule. The expulsion graphs for the M exhibit better correlation than for either the FIN or WAP.

The advantage of the M electrode material is that it is strong enough at low temperatures to limit bulk extrusion, while softening just slightly at higher temperatures to promote localized plasticity at the electrode face [2]. This localized plasticity reduces contact resistance, and thereby heat generation, at the electrode/sheet interface. Due to the proprietary nature of the material, the role of the individual oxides in producing this softening is not known.

5.6 Evolutionary Operation of Weld Schedules

Similar to other industrial processes, weld schedules pass through stages of development. Laboratory results provide a preliminary estimate of feasibility and give ballpark estimates for weld parameters such as weld current, electrode force, and weld time. These laboratory results are incorporated into company process standards that provide weld size requirements and weld set-up recommendations based on the type of steel, coatings, and sheet thicknesses.

Evolutionary Operation (EVOP) is an iterative strategy for approaching the optimum operating conditions of a production process [48, 49, 50]. It is often performed using small changes in parameter settings and large sample sizes [49]. The advantage of EVOP is that it is non-disruptive to the manufacturing process and allows the continued production of saleable product during the procedure. EVOP has been successfully applied to a myriad of industrial processes including the submerged arc welding process [50, 51].

Through the experience of production testing, a methodology has evolved for developing weld schedules based on the elements of EVOP. The methodology relies on moderate expulsion, both in terms of frequency and the amount of metal expelled, as the key determinant for weld schedule feasibility. The goal is to reduce the current level, represented by the start current and stepper rate, to the lowest feasible yet reliable rate. The basic elements of the methodology as applied to current research are:

- running in sequence a set of weld parameters that are minor variants of the currently best-known process;
- recording expulsion data in a readily understood form which leads the way to appropriate action.

The potential benefits are extended electrode life, lower overall energy consumption, and improved weld quality.

The particular welding application is first assessed by identifying the materials and coatings, sheet thicknesses, part fit-up, and any other information related to weldability. The recommended weld parameters are determined from company process standards and any previous laboratory results. The average expulsion current is

determined from at least two current ranges on the welded assembly and is used to establish an appropriate starting current.

A two-variable factorial design is suggested consisting of five operating points, as shown in Figure 43. Point 0 represents the average expulsion current from the current range and an estimated stepper rate based on similar welding applications. The other points represent slight modifications to these values. Trials are conducted at each point of the factorial design and expulsion data are collected. After the trials are completed, the data are analyzed and the most feasible settings are conjectured. The best-known settings become the centre point of the next factorial design as the weld schedule develops.

The mean stepper rate should consider the start current, the maximum current available from the transformer, and the desired number of welds. Following the determination of the mean stepper rate, the stepper schedule is modified in stages. The final stepper schedule should increase the stepper rate for each successive stage to better maintain current density late in electrode life. The final weld schedule is one that produces consistently moderate expulsion while still maintaining weld quality.

The expulsion frequency will vary from trial to trial due to the inherent variability associated with production welding conditions. To ensure that the patterns or trends that arise are solely from the deliberately introduced settings, the order of the individual trials should be randomized. In addition, the final weld schedule should be monitored and evaluated through consecutive production runs. The trial replication assures reproducibility of the results.

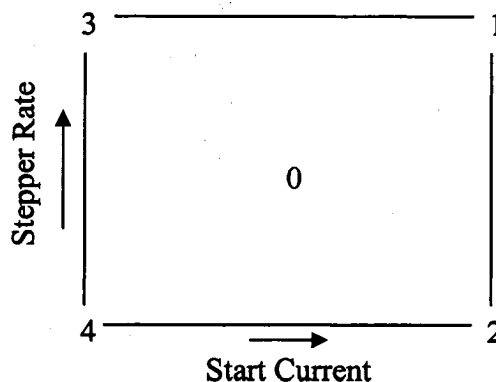


Figure 43: A 2² factorial design for variables start current and stepper rate

The methodology procedure is best served by providing an example application that involves a two-thickness stack-up, 1.1 mm to 1.4 mm, where both parts are hot-dipped galvanized high strength steel. For this example, typical parameters may be:

Electrode force - 2980 N (670 lbf) Weld time - 16 cycles (60 Hz cycles)
Hold time - 2 cycles (60 Hz cycles) Weld current - 10,500 A

The above weld parameters are used to conduct a current range on the actual part. The initial current for the current range is set below the recommended weld current for this application; 8000 A may be considered an appropriate starting point. The current range is conducted by increasing the weld current by 250 A after each successive weld until the first instance of expulsion occurs. A destructive peel test is performed to determine the button sizes of the individual welds. The average expulsion current is determined from at least two current ranges and is selected as the start current for the centre point of the factorial design, as shown in Figure 44.

An approximate stepper rate is determined by considering other applications with similar steel and coating types, and stack-up thickness. This estimated stepper rate, 1.6 A per weld for this example, becomes the stepper rate setting for the centre point. Trials are conducted at each point of the factorial design and the expulsion behaviour is monitored and recorded. In some cases, a high percentage of expulsion will be experienced because conservative values have been chosen. If this occurs, further testing at more conservative start currents and stepper rates is not necessary.

The best-known settings from the first factorial design, 9800 A start current and 1.2 A per weld stepper rate, become the centre point for the following factorial design. The interval between the parameter settings can be reduced for each successive factorial design to further refine the weld schedule. As displayed in Figure 44, the stepper rate interval for the first factorial design is reduced from 0.4 A per weld to 0.2 A per weld. Trials are conducted at each point and the expulsion behaviour is monitored and recorded.

Once a mean stepper rate is determined through testing, the stepper is modified in stages. The initial stepper rate is set approximately 10 percent lower than the mean rate to limit thermal degradation initially and the final stepper rate is set approximately 10 percent higher than the mean rate to maintain current density late in life. If the mean

stepper rate was determined to be 1.4 A per weld, an initial stepper rate of 1.25 A per weld and a final stepper rate of 1.55 A per weld could be used. The expulsion behaviour with the modified stepper schedule is then monitored and recorded through several consecutive production trials.

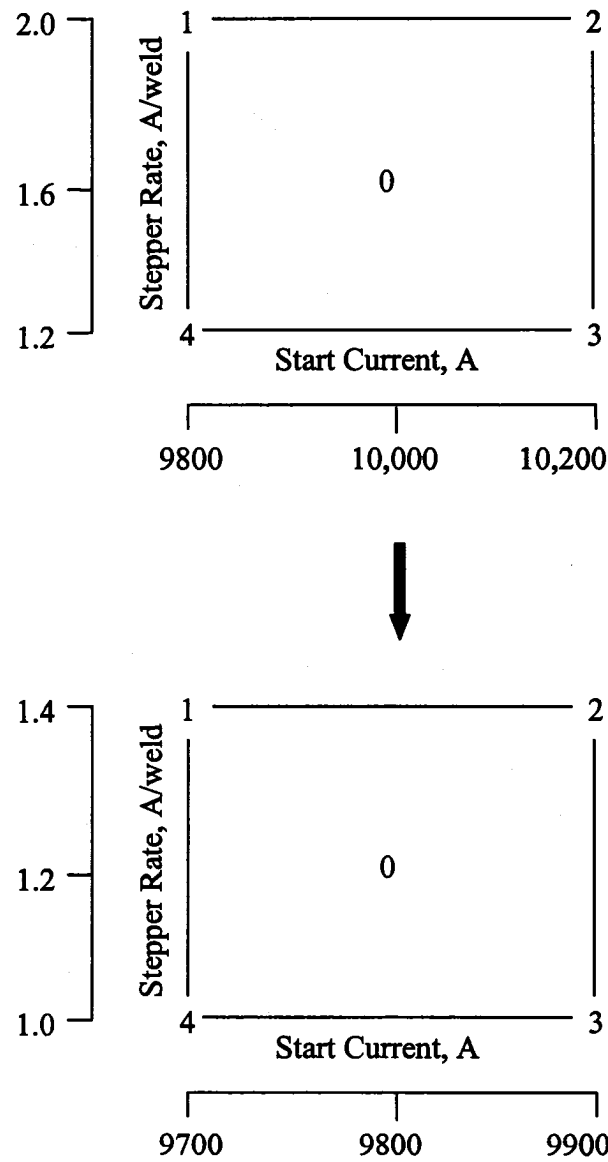


Figure 44: Progression of the factorial design for the example welding application

5.7 Benefits of Evolutionary Operation

The benefits from weld schedule improvement and electrode life extension include cost reductions for electrode replacement and energy consumption. Since energy consumption is directly proportional to the square of welding current, total energy per weld can be dramatically reduced by lower current levels. Furthermore, since extended electrode life has been directly related to lower operating currents [16], the benefits of lower current levels also provide for fewer electrode replacements.

Figure 45 and Table 12 display both graphical and numerical summaries of the daily current requirements, assuming a three-shift operation, for the M-12, FIN-12, and FIN-24 electrodes. The calculations are based on a maximum number of 7500 welds for a 12 hour period and a constant weld time. The numbers indicate that both of the developmental electrodes were able to reduce energy consumption relative to the baseline weld schedule. Most notably, the FIN-12 offered an 18 percent reduction in total amperes consumed per day compared to the baseline weld schedule. Although a detailed power calculation is not available, any reduction in current is expected to result in an energy savings.

Although the FIN was capable of successfully completing a 24-hour trial, the lowest daily current requirements were offered by replacing the FIN electrode every 12 hours. Peterson [52] has also noted that when the face diameter to sheet thickness ratio becomes significantly out of balance, nugget development and weld quality suffer. When considering total energy consumption and weld quality reliability, replacing the FIN every 12 hours offered the most feasible choice. A 12-hour replacement period was selected, rather than a 16-hour period, to reduce scheduling complexity. The electrodes in a 12-hour rotation are replaced at the same time every day as opposed to a 16-hour rotation where they are replaced at different times from day-to-day.

The increased electrode life must be considered relative to the price per electrode. The cost savings associated with fewer electrode replacements must outweigh any added manufacturing costs of a superior electrode. Gallagher [7] noted that the economics of electrodes may be adversely affected by the added manufacturing costs associated with forming fins.

Without information related to electrode and energy costs, it is not possible to offer a more detailed economic analysis. In 2002 it was estimated that the annual savings associated with doubling electrode life, based only on electrode costs and replacement labour, was \$US 20-million for the three North American automakers alone [1]. Since that time, the average price of copper has increased from \$US 0.75 per lb to \$US 3.50 per lb. This represents over a four-fold increase in the price of the base material used to manufacture electrodes. Furthermore, the above value does not represent the significant savings that can be achieved by lower overall energy consumption. Howe [53] has shown that energy costs can be reduced by as much as 50 percent when weld parameters are optimized. Any reduction in energy combined with extended electrode life should result in a significant financial savings for the company.

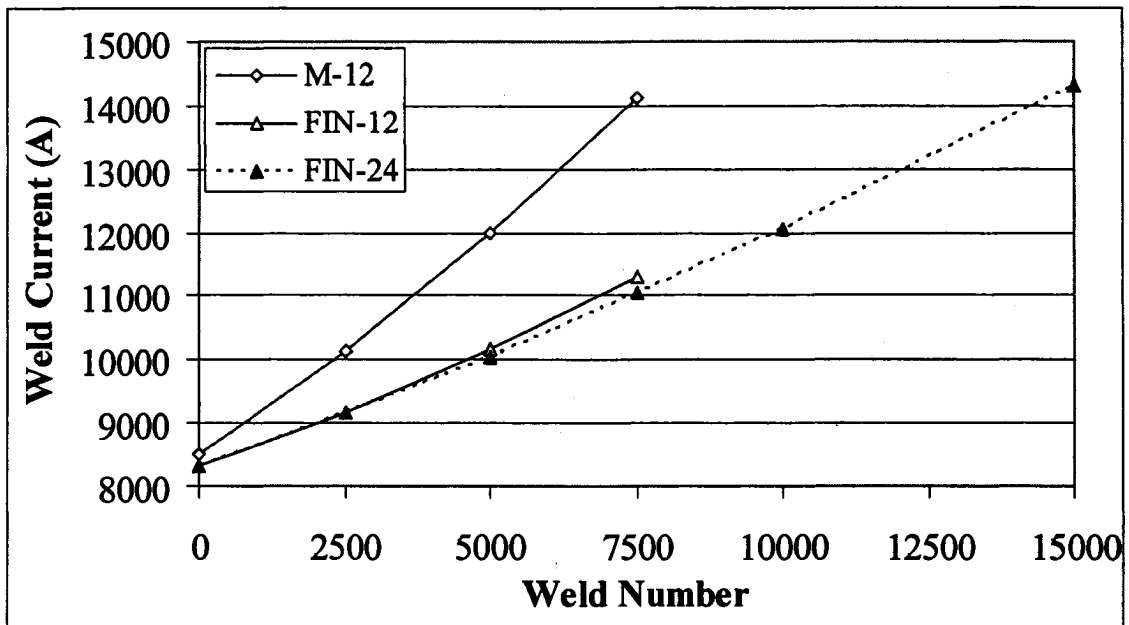


Figure 45: Graph of weld current vs. weld number for the final weld schedules

Electrode	Start Current	Final Current	Total Amps/ 7500 welds $\times 10^6$	Total Amps/ Day (Max) $\times 10^6$	Fraction of Baseline Amps / Day
M-12	8,500	14,125	83.6	167.2	0.94
FIN-12	8,300	11,300	72.9	145.8	0.82
FIN-24	8,300	14,300	N/A	167.0	0.94

Table 12: Summary of weld currents and total amperes for the DCX beta-site trials

VI. CONCLUSIONS AND FUTURE WORK

1. The results of the laboratory and production testing reveal the potential of the M electrode material given its consistent welding performance. This consistency is important in a production environment, where predictability in scheduling and maintenance translate into increased productivity. This multiple-oxide dispersion strengthened copper material is strong enough at low temperatures to limit bulk extrusion, while softening just slightly at higher temperatures to promote localized plasticity at the electrode face, thereby limiting heat generation at the electrode/sheet interface.
2. The evidence of boiled cooling-water that was apparent for the M electrode at a low water flow rate in the laboratory tests was not apparent at the higher water flow rates of the production trials. This observation suggests that the optimum face thickness for electrode cooling is greater than 6 mm for a cooling-water flow rate of 0.5 gpm and that the optimum thickness decreases with higher cooling-water flow rates.
3. The performance of the FIN electrode in the production trials provides evidence that higher cooling-water flow rates are more beneficial for electrodes with cooling properties that enhance convective heat transfer. The addition of fins to the water channel enhanced the rate of convective heat transfer by increasing the water channel surface area and promoting turbulent flow of the cooling-water.
4. Both of the developmental electrodes were able to show repeatable production welding performance in an automotive assembly plant. Most notably, the FIN electrode achieved an 18 percent reduction in total amperes consumed per day compared to the WAP baseline weld schedule. The FIN electrode also completed a successful 24-hour trial, three times the length of the baseline electrode replacement period.
5. A measure of electrode performance when welding galvanized steels is the rate of electrode face enlargement. In this study, improved electrode performance was realized in both the laboratory and production testing when the rate of electrode face enlargement was reduced, thus concurring with this accepted guideline.

6. The current density required to maintain expulsion in the production trials was determined to be on average 86A/mm^2 higher than that required to maintain minimum button size during the laboratory tests.
7. A mixed layer present at the interface of the parting and gamma-brass layers was observed on the electrode face. This mixed layer had an average thickness of $40\ \mu\text{m}$ and was only evident at the central portion of the electrode face. This observation raises the possibility that the mixed layer represents a protrusion, which is an extension of the central portion of the electrode face and has been associated with improved weld consistency.
8. A methodology has been presented to develop weld schedules in production operations without risk to the manufacturing process. It also efficiently compares different electrodes for a given production welding application. The benefits of the methodology include extended electrode life, lower overall energy consumption, and improved weld quality.
9. Improvements in electrode life are only effective within the constraints of production scheduling. For a three-shift operation, 12-hour schedules are preferable to 16-hour schedules despite the ability of the electrode to withstand 16 hours of production welding.

Future work includes investigating the effect of cooling-water flow rate on the performance of the FIN electrode. Computer modeling at various water flow rates would evaluate the performance of the fins on the basis of enhanced heat transfer relative to a no-fin case. Experimental testing of two identical electrodes, with and without fins, at various water flow rates would help determine the optimal cooling conditions for electrode life. The optimization of electrode face thickness and cooling-water flow rate could also be explored in more detail. Transmission electron microscopy of the M electrode material could be conducted to determine the role of the individual oxides in producing the softening at elevated temperatures. The use of the EVOP methodology for other welding applications would further prove its ability to efficiently develop weld schedules in production. Successful production implementation of the M and FIN electrodes to other welding applications would validate the results achieved in this study.

REFERENCES

1. Peterson, W., "A Literature Review of RSW Electrode Wear," Edison Welding Institute Project No.45287CSP, Submitted to USCAR, Southfield, MI, March 28, 2002.
2. Peterson, W., Gould, J., Santella, M., Babu, S., Bowers, R., "Sequential Life Testing of Developmental and Standard Spot Weld Electrode Alloys on Hot-Dipped Galvanized Steel," Edison Welding Institute Project No.46829CAP, Submitted to DaimlerChrysler Corporation, Auburn Hills, MI, August 31, 2004.
3. "Resistance Welding Manual," Revised Fourth Edition, Resistance Welder Manufacturers' Association, Philadelphia, PA, 2003.
4. Cary, H.B., "Modern Welding Technology," Fifth Edition, Prentice-Hall, Upper Saddle River, NJ, 2002.
5. Dickinson, D.W., "Resistance Spot Welding," Metals Handbook, Ninth Edition, Volume 6, Welding, Brazing, and Soldering, American Society for Metals, Metals Park, OH, pp.469-493, 1983.
6. Han, Z., Orozco, J., Indacochea, J.E., Chen, C.H., "Resistance Spot Welding: A Heat Transfer Study," Welding Journal Research Supplement, pp.363s-371s, September 1989.
7. Gallagher, M., "Electrode Wear in Resistance Spot Welding of Galvanized Steel Sheet," M.A.Sc. Thesis, University of Windsor, Windsor, ON, 2003.
8. Irving, B., "Extending Resistance Welding Electrode Life," Welding Journal, pp.58-61, November 2001.
9. "Recommended Practices for Test Methods for Evaluating the Resistance Spot Welding Behavior of Automotive Sheet Steel Materials," American Welding Society Standard D8.9, 2002.
10. "NA Welding Specification WS-5 Weld Testing and Procedures Section A: Resistance Spot Welding," GMNA Controls, Robotics, and Welding, General Motors Corporation, May 2002.
11. "Spot Welding Technical Information," <<http://www.titespot.com/techinfo.html>>, retrieved July 27, 2006.
12. Gould, J.E., "Development of a New Resistance Spot Weldability Test for Coated Sheet Steels," Paper No.10, Sheet Metal Welding Conference IV, AWS-Detroit Section, Southfield, MI, October 1990.

13. Kimchi, M., Gould, J.E., Helenius, A., Heippi, K., Nippert, R.A., "Evaluation of Various Electrode Materials for Resistance Spot Welding Galvanized Steel," Paper No.7, Sheet Metal Welding Conference IV, AWS-Detroit Section, Southfield, MI, October 1990.
14. Gugel, M., "Electrode Wear Mechanisms during the Resistance Spot Welding of Hot-Dipped Galvanized Steel," Ph.D. Dissertation, Michigan Technological University, Houghton, MI, 1995.
15. Gugel, M., White, C., Kimchi, M., "Joining Technologies: Mechanisms of Electrode Wear during Resistance Spot Welding Hot-Dipped Galvanized Steel," Electrode Wear Mechanisms Task Force, Auto/Steel Partnership Technical Report, Southfield, MI, June 1994.
16. Lu, F., White, C., Kimchi, M., "Joining Technologies: Resistance Spot Welding Electrode Wear on Galvannealed Steels," Electrode Wear Mechanisms Task Force, Auto/Steel Partnership Technical Report, Southfield, MI, September 1997.
17. Athwal, B., "Characterization of Electrode Wear Morphology via Sequential Life Testing," M.A.Sc. Thesis, University of Windsor, Windsor, ON, 2005.
18. Gallagher, M., Athwal, K., Bowers, R., "Electrode Wear Characterization in Resistance Spot Welding," Paper No.1-5, Sheet Metal Welding Conference XI, AWS-Detroit Section, Sterling Heights, MI, May 2004.
19. Natale, T.V., "A Review of the Resistance Spot Welding Behavior of Galvanized Steels," Paper No.1, Sheet Metal Welding Conference III, AWS-Detroit Section, Southfield, MI, October 1988.
20. Karagoulis, M., "Control of Materials Processing Variables in Production Resistance Spot Welding," Paper No.B5, Sheet Metal Welding Conference V, AWS-Detroit Section, Detroit, MI, October 1992.
21. Pickett, K., Natale, T.V., "The Effect of Workplace Fit-Up and Electrode Composition on the Resistance Spot Welding Behaviour of Hot-Dip Galvanized Sheet Steel," Paper No.9, Sheet Metal Welding Conference IV, AWS-Detroit Section, Southfield, MI, October 1990.
22. Belleau, C., Kelley, D.K., Marttila W.A., "Some Considerations in the Welding of Automotive Galvanized Steels," Paper No.17, Sheet Metal Welding Conference I, AWS-Detroit Section, Dearborn, MI, October 1984.
23. Ohrman, P. D., "Precoated Steel Sheet," Metals Handbook, Ninth Edition, Volume 1, Properties and Selection: Irons, Steels, and High-Performance Alloys, American Society for Metals, Metals Park, OH, pp.167-176, 1978.

24. "Galvannealed Coatings: How Do They Differ from Galvanized?" <http://www.steelmillsoftheworld.com/activities/datacenter/G_Note5.pdf>, retrieved March 27, 2006.
25. Burton, B.P., Perrot, P., "Fe-Zn," ASM Handbook, Volume 3, Alloy Phase Diagrams, ASM International, Materials Park, OH, pp. 2.206, 1992.
26. Gould, J.E., Peterson, W.A., "Electrode Life Parametric Studies," Paper No.3, Sheet Metal Welding Conference III, AWS-Detroit Section, Southfield, MI, October 1988.
27. Upthegrove, W.R., Key, J.F., "A High Speed Photographic Analysis of Spot Welding Galvanized Steel," Welding Journal Research Supplement, pp.233s-244s, May 1972.
28. Howe, P., Kelley, S.C., "Coating Weight Effect on the Resistance Spot Weldability of Electrogalvanized Sheet Steels," Welding Journal Research Supplement, pp.271s-280s, December 1988.
29. Freytag, N. A., "A Comprehensive Study of Spot Welding Galvanized Steel," Welding Journal Research Supplement, pp. 145s-156s, April 1965.
30. Friedman, L.M., McCauley, R.B., "Influence of Metallurgical Characteristics on Resistance Welding of Galvanized Steel," Welding Journal Research Supplement, pp.454s-462s, October 1969.
31. Matsuda, H., Matsuda, Y., Kabasawa, M., "Effects of Aluminium in the Zn Coating on Electrode Life in Welding Galvanized Steel Sheet," Welding International (UK), Vol.10, No.8, pp.605-613, 1996.
32. Gagné, M., Baril, E., Bélisle, S., L'Espérance, G., Boutin, E., Hong, B., Goodwin, F., "Distribution of Aluminum in Regular Hot-Dip Galvanized Steel Coatings," Zinc-Based Steel Coating Systems: Production and Performance, The Minerals, Metals and Materials Society, pp.229-238, 1998.
33. Natale, T., Dilay, W., Chang, D., "Resistance Spot Weldability of Thin Gauge Zinc Coated Sheet Steel," Paper No.16, Sheet Metal Welding Conference I, AWS-Detroit Section, Dearborn, MI, October 1984.
34. Pickett, K.M., Mishowski, J.J., Gould, J.E., "The Effect of Total Iron Content and Intermetallic Phase Distribution on the Resistance Spot Weldability of Hot Dip Galvanized Sheet Steel," Paper No.A2, Sheet Metal Welding Conference V, AWS-Detroit Section, Detroit, MI, October 1992.

35. Howes, S.W., Lake, J.S.H., "Degradation of Electrodes When Resistance Welding Metallic Coated Sheet Steels," Paper No.10, Sheet Metal Welding Conference III, AWS-Detroit Section, Southfield, MI, October 1988.
36. Miodownik, A.P., "Cu-Zn," ASM Handbook, Volume 3, Alloy Phase Diagrams, ASM International, Materials Park, OH, pp. 2.182, 1992.
37. Dong, P., Kimchi, M., "Thermomechanical Analysis of Electrode Wear Mechanisms," Paper E5, Sheet Metal Welding Conference VII, AWS-Detroit Section, Troy, MI, October 1996.
38. Holliday, R., Parker, J.D., Williams, N.T., "Relative Contribution of Electrode Tip Growth Mechanisms in Spot Welding Zinc Coated Steels," Welding in the World, Vol.37, No.4, pp.186-193, 1996.
39. Wist, J., White, C., "Metallurgical Aspects of Electrode Wear during Resistance Welding of Zinc Coated Steels," Paper No.6, Sheet Metal Welding Conference IV, AWS-Detroit Section, Southfield, MI, October 1990.
40. Nadkarni, A., Solomon, R., "Influence of RSW Tip Geometry on Tip Performance Welding Zinc Coated Steel," Paper No.A5, Sheet Metal Welding Conference V, AWS-Detroit Section, Detroit, MI, October 1992.
41. De, A., Dorn, L., Gupta, O.P., "Analysis and Optimisation of Electrode Life for Conventional and Compound Tip Electrodes during Resistance Spot Welding of Electrogalvanised Steels," Science and Technology of Welding and Joining, Vol.5, No.1, pp.49-57, 2000.
42. Gugel, M.D., Wist, J.A., White, C.L., "Comparison of Electrode Wear in DSC Electrodes Having Different Hardness," Paper No.A3, Sheet Metal Welding Conference V, AWS-Detroit Section, Detroit, MI, October 1992.
43. Kimchi, M., Gould, J.E., Nippert, R.A., "The Evaluation of Resistance Spot Welding Electrode Materials for Welding Galvanized Steels," Paper No.8, Sheet Metal Welding Conference III, AWS-Detroit Section, Southfield, MI, October 1988.
44. "Resistance Spot Welding Automotive Components," DaimlerChrysler Corporation Process Standard 9471.
45. Czitrom, V., Spagon, P.D., "Statistical Case Studies for Industrial Process Improvement," American Statistical Association and the Society for Industrial and Applied Mathematics, pp.63, 1997.

46. Kim, E., Eagar, T., "Transient Thermal Behavior in Resistance Spot Welding," Paper No.2, Sheet Metal Welding Conference III, AWS-Detroit Section, Southfield, MI, October 1988.
47. Çengel, Y., "Heat Transfer: A Practical Approach," McGraw-Hill, USA, pp.382, 1998.
48. Box, G., Draper, N., "Evolutionary Operation: A Statistical Method for Process Improvement," John Wiley & Sons, Inc., USA, 1969.
49. Lynch, D., "EVOP Design of Experiments," Proceedings, 2003 SAE World Congress, Detroit, MI, March 2003.
50. Srisupinanont, C., Keith, R., Ham, I., "Optimization of Welding Conditions Using EVOP," Proceedings, American Institute of Industrial Engineers, Annual Conference and Convention, pp.286-293, May 1977.
51. Hunter, W.G., Kittrell, J.R., "Evolutionary Operation: A Review," Technometrics, Vol.8, No.3, pp. 389-397, August 1966.
52. Peterson, W., "Long-Life Electrodes for Resistance Spot Welding of Aluminum Sheet Alloys and Coated High-Strength Steel Sheet," U.S. Automotive Materials Partnership, Semi-Annual Progress Report, March 31, 2005.
53. Howe, P., "Spot Welding Parameters Optimization for Achieving Electrical Power Consumption Reduction and Improving Weld Quality," Paper No.18, Sheet Metal Welding Conference IV, AWS-Detroit Section, Southfield, MI, October 1990.

VITA AUCTORIS

NAME Jeremy Caron

PLACE OF BIRTH Chatham, Ontario

DATE OF BIRTH November 4, 1981

EDUCATION

Ontario Secondary School Diploma
Belle River District High School
Belle River, Ontario
2000

Bachelor of Applied Science
Honours Mechanical Engineering - Materials Option
University of Windsor
Windsor, Ontario
2004

Master of Applied Science
Engineering Materials
University of Windsor
Windsor, Ontario
2006